MULTI-SENSOR SSC RETRIEVAL, A CASE STUDY OVER THE YANGTZE RIVER ESTUARY

XIN SU
February, 2014

SUPERVISORS:
Prof. dr. ing. W. (Wouter) Verhoef
Dr. ir. J. (Joris) Timmermans

MULTI-SENSOR SSC RETRIEVAL, A CASE STUDY OVER THE YANGTZE RIVER ESTUARY

XIN SU
Enschede, The Netherlands, February, 2014

Thesis submitted to the Faculty of Geo-Information Science and Earth Observation of the University of Twente in partial fulfilment of the requirements for the degree of Master of Science in Geo-information Science and Earth Observation.
Specialization: Water Resources and Environmental Management

SUPERVISORS:
Prof. dr. ing. W. (Wouter) Verhoef
Dr. ir. J. (Joris) Timmermans

THESIS ASSESSMENT BOARD:
Dr. Ir. M.S. Salama (Chair)
Dr. M.R. Wernand (External Examiner, Royal Netherlands Institute for Sea Research, Texel)

ABSTRACT

The amount of suspended sediment plays an important role in the morphological development of the Yangtze River estuary. The sediment load in the Yangtze River estuary decreased dramatically in the half past century due to upstream dam constructions and other human activities. Such change leads to a fundamental environmental and geomorphological impact on the Yangtze delta and consequently influences the agriculture and economy in this area. So it is important to investigate how the suspended sediment concentration (SSC) changed in the Yangtze River estuary. Several studies have therefore focused attention on retrieval of SSC.

Most of the researches have focused on using MERIS imagery, as this sensor was specifically designed for retrieving ocean parameters. While these researches have successfully retrieved SSC, extra research should be performed due to the limited revisit frequency of MERIS. MERIS only has a revisit time of three days while SSC changes every day. Therefore it is necessary to increase the frequency of observation to better monitor SSC variations. This can be done by using multiple satellites. However, using a multi-sensor approach requires that the retrieval of SSC is homogeneous for the different sensors.

In the retrieval of SSC, the most important steps are 1) atmospheric correction, and 2) ocean parameters retrieval from the reflectances acquired in step 1. Correct atmospheric correction is important because more than 90% of radiance received by the sensor is contributed by the atmosphere.

Within the atmospheric correction, haze is especially important because firstly, the atmospheric radiance makes lots of contribution to the TOA radiance. Secondly, in most cases the haze is spatially variable, so we cannot consider it as homogeneous. However, most of the research is taken the haze as homogeneous and consequently this leads to increased uncertainties in the SSC product.

The aim of this research is to improve the quality of SSC products over the Yangtze River estuary using a multi-sensor approach that integrates both atmosphere correction and water parameter retrieval.

In the research, we developed a new model that enables the correction of spatially variable haze retrieval of high sediment concentration through application of the atmospheric correction and the Duntley water radiative transfer model on the two different sensors MODIS and MERIS.

Firstly, we analysed MODIS level 1 images. We found that within MODIS images, in many bands the signal for sediment retrieval is saturate due to high sediment loads. It turned out that these images cannot be used for sediment retrieval in my study area. Fortunately, we found that MERIS images do not have these problems and therefore could be used in this research.

We first used MERIS L1b images to perform the atmospheric correction by using MODTRAN and then compared with the result with MERIS L2 operational product provided by case-2 regional processor (C2RP). From the results, we conclude that the atmospheric correction result by the MODTRAN model has a higher accuracy for the Yangtze River estuary. Using atmospherically correct imagery by the MODTRAN model we retrieve SSC by using the Duntley model. In this way we can get higher quality SSC products.

ACKNOWLEDGEMENTS

First of all, I should thank my father and my mother sincerely to support me all the time and to help me realize my dream.

I would like to appreciate ITC and Chang'an University to give me this opportunity to study at the Water Resources department.

I wish to express my honest gratitude to my supervisors, Prof. dr. Wouter Verhoef and Dr. Joris Timmermans, since they are teaching me a lot with patience, encouraging me all the time and giving me many useful suggestion and critical comments during my research. If I was without them, I could not finish my research at all. I also want to thank Dr. Suhyb Salama for helping me and giving me useful suggestions.

I appreciate Mr. Xiaolong Yu, PhD student and Bingbing Wang, PhD student at the Water Resources department, who shared insightful knowledge with me and helped me a lot during the research.

I am also grateful to all my classmates, Mr. Asmelash Abreha, Mr. Teshale Danbara, Mr. Amr El- Zehairy, Mr Mastawesha Engdaw, Ms Edika Masisi, Mr Jonathan Mwania, Mr Mahmoud Soheili and Ms Chenyang Zhang, for giving me ideas and happiness during my MSc study. I wish our friendship will go on and everybody can enjoy their further life.

Thanks to all ITC staff, especially to all staff in WREM during the lectures. I learned a lot and it will help me in the future.

Too many thanks that I cannot say one by one. I thank to all my friends who I met in the Netherlands. I spent a really wonderful time with you here.

TABLE OF CONTENTS

LIST OF FIGURES

LIST OF TABLES

ACRONYMS

SSC Suspended Sediment Concentration
CZCS Coastal Zone Color Scanner
MODIS Moderate Resolution Imaging Spectroradiometer
MERIS Medium Resolution Imaging Spectroradiomater
SPM Suspended Particulate Matters
SERT Semi-Empirical Radiative Transfer
MDP Multispectral Data Projection
LUTs Look-Up Tables
CDOM Colored Dissolved Organic Matter
MIM Matrix Inversion Method
SIOPs Specific Inherent Optical Properties
RT Radiative Transfer
TOA Top Of the Atmosphere
RMSE Root Mean Square Error
C2RP Case-2 Regional Processor

1. INTRODUCTION

1.1. Background

Suspended Sediment Concentration (SSC) in coastal waters plays an important role in estuary and coastal environments. It influences not only the water quality but also the geomorphologic evolution in the estuary area. In most coastal areas SSC tends to be high in concentration and also highly spatially variable, due to the collective impacts of river discharge, tides, wind-driven waves, and currents (Li et al., 2012). A better understanding of the SSC distribution is critical for the analysis of geomorphologic evolutions, rates of erosion and sedimentation, riverine flux, and aquatic environments (Shen, Verhoef, et al., 2010).
The Yangtze River, ranking fourth in terms of sediment load in the world, has huge amounts of average annual water and sediment discharges: 9.04×10^{11} m^3 and 4.35×10^8 tons (at Datong, from 1951 to 2000) respectively (Chen et al., 2003). The Yangtze sediment load entering the estuary has decreased dramatically over the past half century, under the influence of anthropogenic and natural impacts, such as constructions of dams and reservoirs, soil and water conservation practices (Chu et al., 2013). This has a fundamental impact on the environmental and geomorphological development of the Yangtze delta (Dai & Lu, 2013). It is therefore important to investigate these changes of SSC in the Yangtze River estuary.

1.2. Study area

The Yangtze River is one of the largest rivers in the world; it ranks as the third largest River in length, fifth largest in water discharge, and fourth largest in sediment load. It runs into the East China Sea nearby Shanghai. The Yangtze estuary is located on the east coast of China (see Fig. 1). The suspended sediment concentrations have a wide range from 20 to 2500 mg/l (Shen, Verhoef, et al., 2010) and are spatially and temporally variable in the Yangtze River estuarine and coastal waters. My study area can be divided into seven parts shown in Fig. 2. Based on investigations for SSC distribution in the Yangtze River estuary, these seven parts can be divided again into five situations:
1) In area (1) South Branch, the moderately turbid water, located 121°E- 121°55'E, with an average between 100 and 250 mg l^{-1};
2) In area (2) South Passage, (3) North Passage and (4) North Harbor, the hyper turbid water, located at 121°55'E–122°15'E, with an average between 500 and 900 mg l^{-1} and a maximum value up to 2,500 mg l^{-1} in the South Passage;
3) In area (5) Hangzhou Bay, the super turbid water, ranging between 500mg/L and 1000mg/L;
4) In area (6) a transitional area, the highly turbid water, the area is located at 122°15'E–122°30'E, with an average between 250 and 500 mgl^{-1};
5) In area (7) clean water, low turbid waters, located at 122°30'E – 124 E, with the SSC level below 100 mg l^{-1}(He et al., 1999).

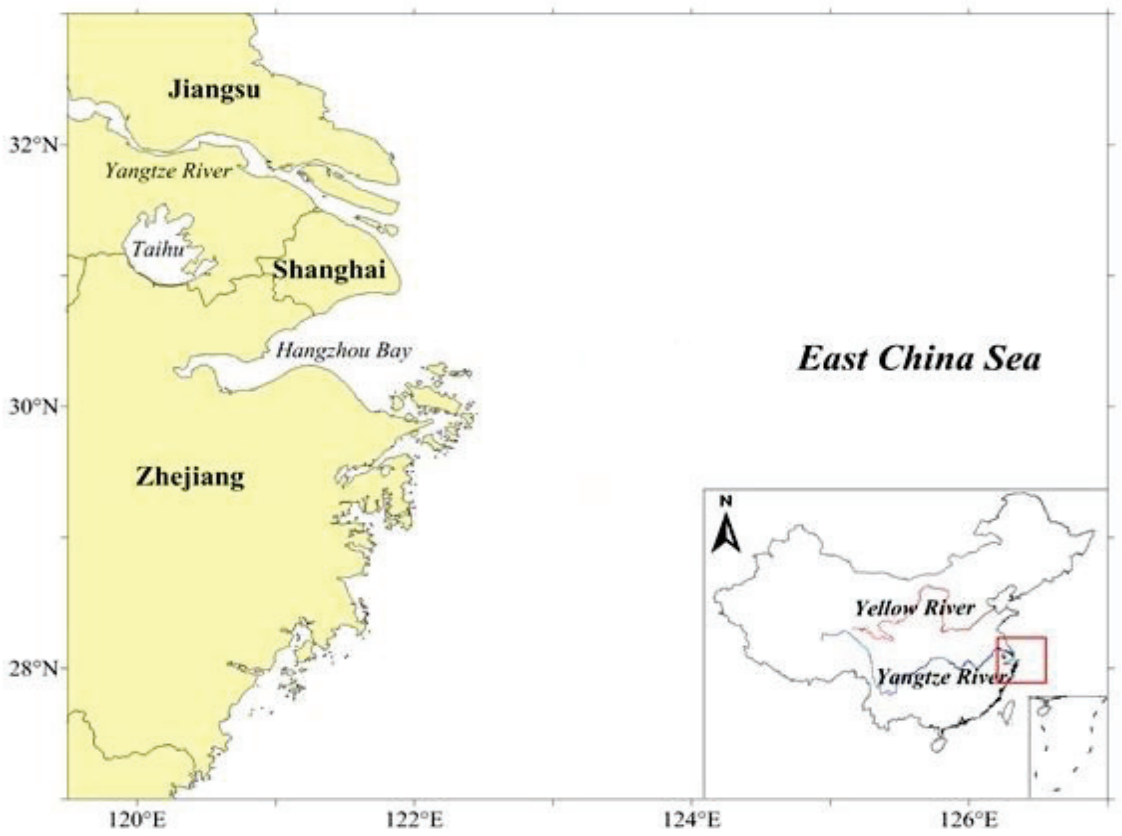

Figure 1 Location of the Yangtze River estuary

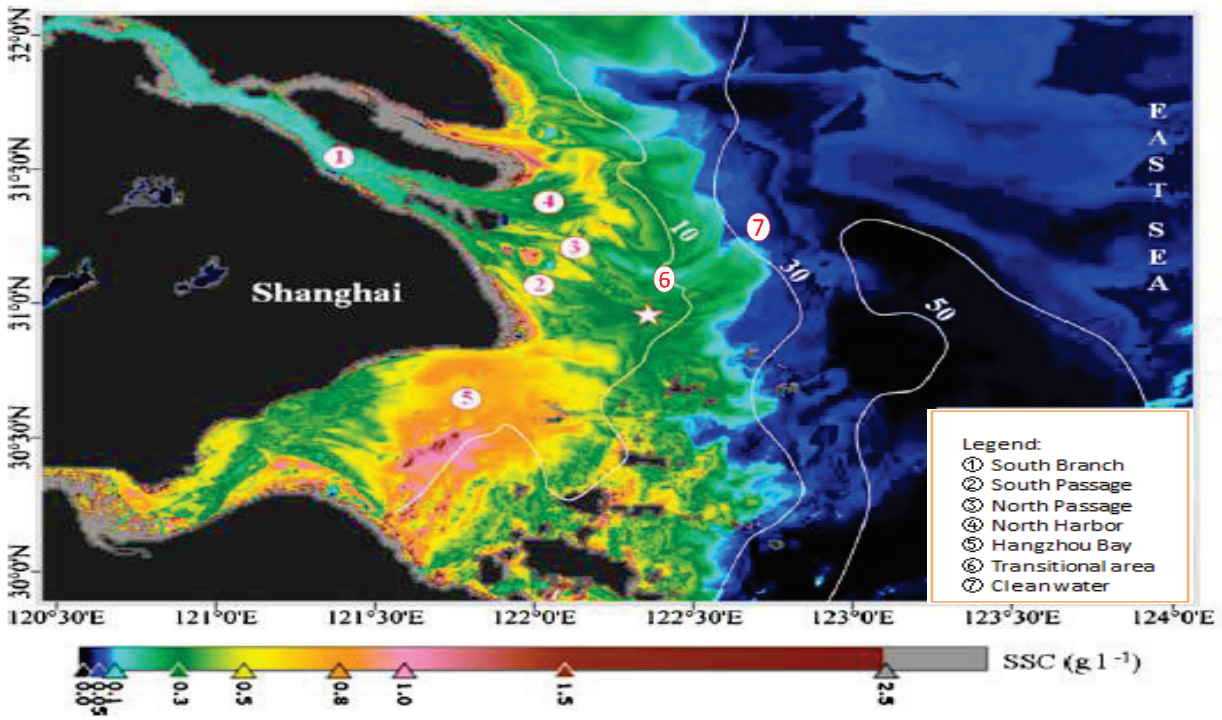

Figure 2 Mapping of SSC retrieved from the MERIS data of April 25, 2008 over the Yangtze estuary and coast (Shen, Verhoef, et al., 2010)

1.3. Remote sensing

Traditional measurements of suspended sediment concentrations (SSC) are in-situ measurements that take samples from the rivers. This method is expensive and time-consuming. And therefore it cannot provide continuous records of SSC (Wang & Lu, 2010).
At present, remote sensing is the only method that can provide spatially dense observations at a high frequency. Hence, this can help in obtaining a better understanding of spatially and temporally variable SSC in the ocean.
The satellites that have been used for water quality analysis can be divided into two types: 1^{st}generation and 2^{nd}generation satellite sensors.

(1) The first satellite-borne ocean color sensor launched (October 1978) was the Coastal Zone Color Scanner (CZCS). This satellite was successfully operated, and triggered a revolution in the way oceanographers look at the marine environment (Barale, 1999). However, it also had some constraints in its low spectral resolution, sensitivity and radiometric accuracy.
(2) Therefore, the second generation sensors were created to circumvent these limitations (Bricaud et al., 1999). In particular, NASA's Moderate Resolution Imaging Spectroradiometer (MODIS) on the Aqua and Terra satellite platforms and ESA's Medium Resolution Imaging Spectroradiometer (MERIS) on the Envisat-1 satellite platform are typical 2^{nd} generation sensors that can be used for ocean color observations. Although the ENVISAT satellite was suddenly lost on April 8, 2012 after its tenth year in orbit, the follow-on Sentinel-3 satellite will carry an Ocean and Land Color Instrument (OLCI) similar to MERIS and is planned to be launched in 2015 (Malenovský et al., 2012)

Since in remote sensing the satellite sensor only observes reflected/transmitted radiation, for all satellite sensors a link must be found between water properties and the measured radiation at the top of the atmosphere. Most methods derive the optical properties in water from the spectral radiance using different methods. In recent years, an increasing number of retrieval methods have been created for ocean color observation. In the particular case of the Yangtze River, many researches (Salama & Shen, 2010; Shen & Verhoef, 2010; Shen, Verhoef, et al., 2010) have been completed using a variety of algorithms. According to these researches, two main factors to determine the accuracy of retrieval quality were found. These are

1) The quality of the atmospheric correction;
2) The algorithm of SSC retrieval from surface reflectance data.

Both will be discussed in the following sections.

1.4. Atmospheric correction

Atmospheric correction aims to remove the effects that result from scattering and absorption in the atmosphere from the measured top-of-atmosphere radiances (Schroeder et al., 2007) . In remote sensing of ocean color, in many cases less than 10% of the observed radiance is reflected at the sea surface, while

90% of the radiance signal is caused by the atmospheric scattering. Atmospheric correction has a large impact on the quality of the SSC retrieval. Only after the atmospheric correction has been performed, water leaving reflectance can be linked to water optical properties to retrieve SSC.

This has led to many researches trying to improve the atmospheric correction of remote sensing data. Gordon and Wang (1994) performed an ocean colour standard algorithm of atmospheric correction that is based on the assumption of zero water -reflectance in the NIR spectral region. They could therefore derive the atmospheric reflectance from the NIR bands and therefore use it to derive the SSC from the other bands. However, this method is invalid for Case 2 waters, which contain much sediment, because the water reflectance in the NIR bands cannot be ignored for these waters. Salama and Shen (2010) developed, on the basis of the GSM model and the Gordon model, a coupled method to retrieve SSC by estimating the backscattering coefficient of suspended particulate matter(SPM) and aerosol reflectance simultaneously from NIR reflectance. But this method is sensitive to the value of aerosol optical thickness. Meanwhile, this method is not suitable for highly turbid waters. In response to this, Shen, Verhoef, et al. (2010)created another method for areas with high turbidity. This method involved an independent atmospheric correction based on the radiative transfer model MODTRAN4 and the SERT (semi-empirical radiative transfer) model to retrieve SSC. According to the validation results, the SERT model for SSC retrieval can be used for high turbidity waters. However, they found that outputs were sometimes overestimated due to the spatially variable atmospheric haze, which is not considered in the homogenous atmosphere of the MODTRAN model. For spatially variable haze, an image-based linear regression model for haze correction was proposed by Ji (2008), but this is not suitable for turbid water. Finally, Shen and Verhoef (2010) proposed to use a multispectral data projection (MDP) method to suppress local haze variations in the Yangtze River estuary before the standard atmospheric correction. By application of this MDP method, using the same atmospheric correction model MODTRAN4 and SERT model , the quality of the SSC retrievals is higher than without this method (Shen, Verhoef, et al., 2010) ,due to the suppression of local haze variations. This method has only been validated with MERIS data. Up to now, no studies have applied the method based on spatially variable haze over turbid waters for MODIS data (Hu et al., 2000; Schroeder et al., 2007).

1.4.1. MODTRAN model

MODTRAN serves as the U.S. Air Force (USAF) standard moderate spectral resolution radiative transport model for wavelengths extending from the Thermal Infrared (TIR) through the visible and into the ultraviolet (0.2 to 10,000.0 μm)(Berk et al., 2011). In MODTRAN4, options that include azimuthal dependencies in the calculation of DISORT solar scattering contributions, and Scaling options for water vapour and ozone column amounts are provided (Berk et al., 1999). MODTRAN5 in this study has been treated as a black box and an "interrogation" technique has been applied in order to derive atmospheric parameters from the outputs of three different MODTRAN runs.

1.4.2. C2R processor

The Case-2 regional (C2R) processor is provided in the form of a plug-in that can be carried out by users in the software package BEAM, which was developed for MERIS L1B data in the MERIS regional coastal and lake Case 2 water project funded by ESA(Doerffer & Schiller, 2008). This processor contains a

procedure for atmospheric correction and procedures for determining inherent optical properties that outputs MERIS L2 products with reflectance, inherent optical properties (IOPs), and water quality parameters such as Chl-a and TSM for those special or regional cases such as coastal and different lake waters(Duan et al., 2012). However, the C2R processor may be invalid for very high chlorophyll-rich waters like some Eutrophic lakes(Doerffer & Schiller, 2007) and for highly turbid water (Shen, Verhoef, et al., 2010). More detailed information on the C2R processor is provided in section 2.3.5.

1.5. SSC retrieval

The algorithm of SSC retrieval is aimed at linking the optical properties of water with the water leaving reflectance using radiative transfer theory so as to parameterize the SSC using water optical properties. An appropriate retrieval algorithm is the key step to determine the retrieval quality directly. Water optical properties are usually described by means of a backscattering coefficient and an absorption coefficient. On the basis of this, water can be classified as Case 1 waters and Case 2 waters.

(1) Clearer waters which are characterized as Case 1 waters only contain phytoplankton and related particles and products (Jorgensen, 1999).

(2) Case 2 waters not only contain phytoplankton and related particles, but also colored dissolved organic matter (CDOM) and inorganic suspended particulate matter (SPM) (Schroeder et al., 2007). In Case 2 waters, the components are independent of each other and not influenced by the phytoplankton. Therefore, most estuarine and coastal waters can be classified as Case 2 waters （Gordon and Morel, 1983) that are highly turbid with high suspended sediment concentrations. The Yangtze River estuary belongs to the Case 2 waters with a very high sediment concentration.

Up to now, many researches have been completed for SSC retrieval in Case 2 waters. For satellite estimates of high SSC, empirical algorithms, like the algorithm of the ratio of the MODIS red band to the near infrared (NIR) band developed by Doxaran et al. (2002); Doxaran et al. (2009). This method could be just suitable for high SSC in a limited range and would lead to larger errors for low SSC. Another semi-analytical algorithm developed by Fettweis et al. (2007) was applied for investigating the relationships among absorption coefficients, backscattering coefficients and water leaving reflectance related to SSC. However, this method was mainly suitable for low or moderate SSC waters. Salama and Shen (2010) used a semi-analytical model, based on the Gordon model and the GSM model (Gordon et al., 1988) to retrieve SSC for the Yangtze River estuary. However, these models are not valid for highly turbid waters. Therefore, Shen, Verhoef, et al. (2010) used the SERT model for the Yangtze River estuary, that is based on the two-stream K-M model (Kubelka & Munk, 1931). The K-M model is more suitable for highly turbid waters. However, this only considers the two diffuse (upward and downward) streams. Especially under sunny conditions, the SSC retrieval value will be overestimated. This can be prevented by taking into consideration the solar incident radiation. A possible implementation of this solution is by using the Duntley equations (Duntley, 1942). These equations describe the radiative transfer using two diffuse streams with direct solar radiation added. The hemispherical upward and downward diffuse streams are similar to the K-M model, but also the direct radiation from the sun is added to the system of differential equations. The Duntley equations have not been used in the previous studies for the Yangtze River estuary.

1.6. Summary of research problems

In investigating the SSC for the Yangtze River estuary the following research problems have been identified:

1. Atmospheric correction procedures dealing with spatially variable haze, and their validation for different satellite sensors.
2. The K-M model is suitable for high sediment concentrations, but may provide lower accuracies under sunny conditions. This could be solved by implementing the Duntley model

Summarized, I have used both the surface and the atmospheric correction model to retrieve SSC, based on assuming spatially variable haze and using the Duntley model for water radiative transfer.

1.7. Objectives

My main objective was to improve the quality of SSC products over the Yangtze River estuary, China, using simultaneous atmospheric correction and SSC retrieval model. This can be broken down into several specific sub-objectives.

1. To investigate the availability of the MODIS and MERIS satellites imagery
2. To create a coupled model for SSC retrieval from satellite imagery, dealing with
   a) Atmospheric correction
   b) SSC retrieval
3. To investigate the quality of the method by evaluating the SSC products

1.8. Research questions

1.8.1. How to reduce revisit time by finding good images from MODIS and MERIS?

1.8.2. How to design and implement an algorithm to derive the SSC from satellite imagery using the coupled model?

1.8.3. To what extent is the quality of the products improved by using the new method?

1.9. Hypothesis

We assume that this model can improve the quality of SSC products.

2. METHODOLOGY AND DATA REQUIREMENTS

2.1. Method Overview

The following processing steps were undertaken:

1. Preparation of two sensors imageries
2. Atmospheric correction of MERIS images

2.1 Sensitivity analysis with MODTRAN

2.2 Atmospheric correction by MODTRAN

2.3 C2RP and comparing these two methods

3. SSC retrieved by Duntley model and generation of SSC products

3.1 Determining SIOPs

3.2 SSC retrieved and generated two SSC products by using two different atmospheric correction models: the MODTRAN model and the C2R processor

4. Comparison between two SSC products from two atmospheric correction models

The main flow chart of my research is illustrated in Fig. 3 to show how to implement the sub-objectives 2 and 3.

1. In the orange part, the atmospheric correction is shown and this will be discussed in section 2.3.
2. In the purple part, the SSC retrieval algorithm is shown and this will be discussed in section 2.4. In the orange part and the purple part, the sub-objective 2 can be solved to retrieve the SSC values from MERIS imagery
3. In the blue part, the sub-objective 3 could be solved to evaluate the quality of this model by comparing two SSC products by different atmospheric correction models, which will be discussed in section 2.5.

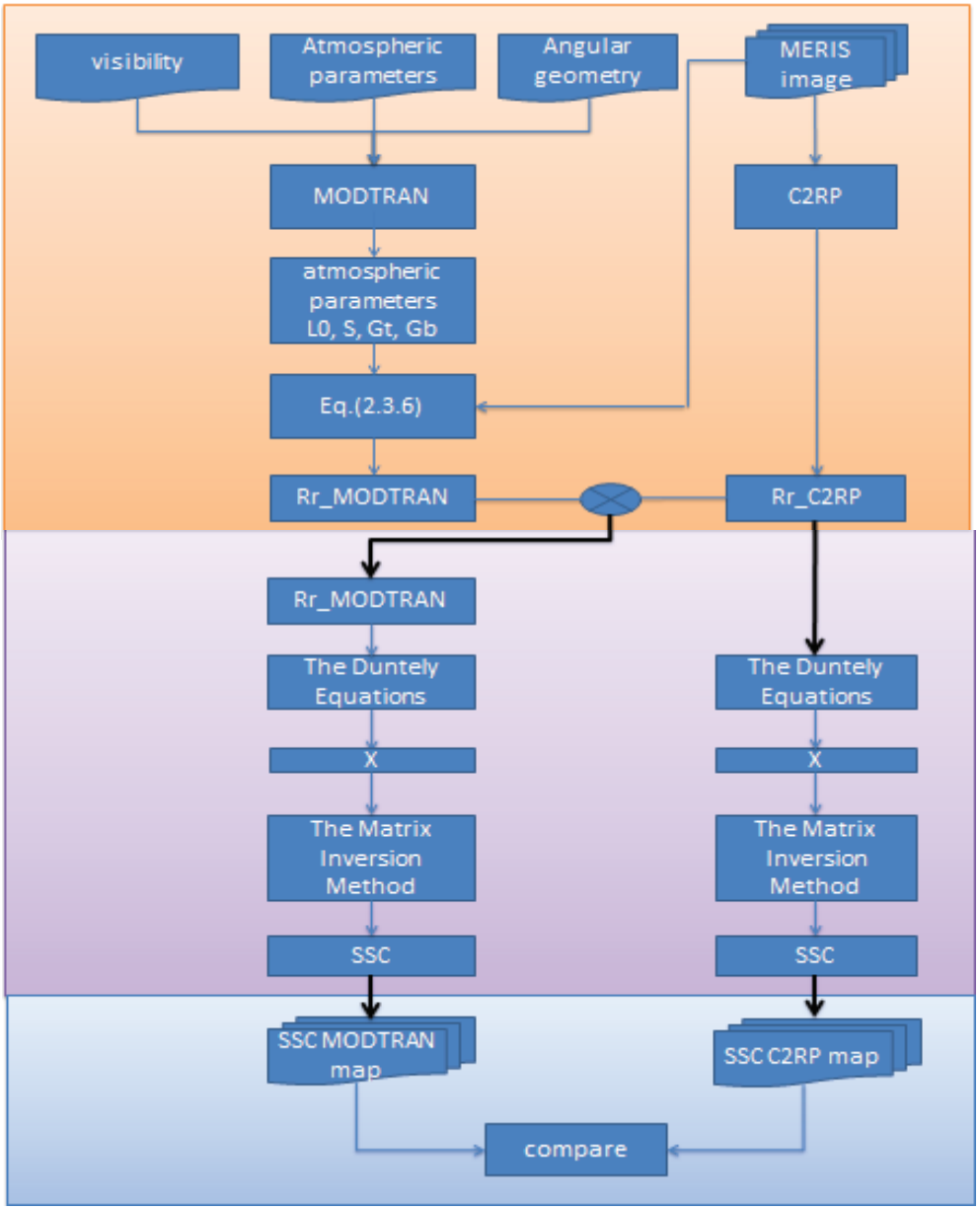

Figure 3 The main flow chart of this research

2.2. Satellite data set

2.2.1. MODIS imagery acquired

The first sensor is the Moderate Resolution Imaging Spectroradiometer (MODIS) on USA Aqua and Terra satellite platforms that also provide channels for ocean color monitoring. MODIS has in total 36 bands with spatial resolutions of the first two bands 250 m, 3-7 bands 500 m and the others 1000 m. Appropriate bands from the 8-19 bands (405 nm- 965 nm) were chosen for the SSC retrieval. MODIS passes the Yangtze River two times per day, once in the morning and once during the night. MODIS Terra and Aqua level 1 calibrated radiance images were chosen. Table 1 shows the MODIS spectral bands below:

Table 1 MODIS spectral bands and applications

Primary use	Band number	Bandwidth (nm)
Ocean color/ phytoplankton/ biogeochemistry	8	405 - 420
	9	438 - 448
	10	483 - 493
	11	526 - 536
	12	546 - 556
	13	662 - 672
	14	673 - 683
	15	743 - 753
	16	862 - 877
Atmospheric water vapor	17	890 - 920
	18	931 - 941
	19	915 - 965

1. MODIS spectral bands chosen

4 scenes were chosen from Aqua and the other 4 scenes were chosen from Terra without clouds between 2005- 2008. These bands 8-19 can be used for ocean color retrieval and atmospheric water vapor in my research .The spectral resolution is 1000m. Table 2 shows the dates of images that were chosen below:

Table 2 MODIS images dates

	Terra	Aqua
Dates	23 July 2005 2:35	7 April 2007 5:05
	27 August 2006 2:35	26 July 2007 5:15
	29 July 2007 2:35	5 July 2008 5:10
	06 July 2008 2:35	14 July 2008 5:05
Band (-)	8 – 19 (405 – 965 nm)	
Resolution (m)	1000 m	

2. Date quality investigation

When choosing appropriate images, the scenes should not be cloudy in the study area. The over- pass time should be close to those of MERIS images in order to get the best matchup. In this research, all these 8 scenes were chosen without clouds over the Yangtze River and the overpass of the MODIS Terre images are very close to MERIS overpass time. The MERIS will be discussed in section 2.2.2.

2.2.2. MERIS imagery acquired

The second sensor is the Medium Resolution Imaging Spectroradiometer (MERIS) on the Envisat-1 satellite platform of the European Space Agency (ESA) that was primarily intended for ocean, coastal and continental waters remote sensing and consequently has a lot of valuable information. MERIS has in total 16 bands that can be transmitted to the ground segment with two spatial resolutions, Reduced Resolution

(1040m * 1200m) and Full Resolution (260m * 300m). However, only 15 bands from 412.5 nm to 900 nm can be used for ocean color observation. MERIS has a revisit time of three days over the Yangtze River estuary at around 10 a.m. in local time. Here, MERIS FR level 1b images are resampled on a path-oriented grid, with pixel values having been calibrated to match the Top of the Atmosphere (TOA) radiance. The MERIS Level 1 products provide the radiance as measured by the instrument. The bands can be used to construct colour composite images, either giving a photographic impression or highlighting certain thematic features of the Earth, and they are input to processing algorithms to derive Level 2 products. The MERIS FR L1B image on April 25 2008 was appropriately chosen in my case. Table 3 shows the spectral bands of MERIS.

MERIS L1 B image provides radiance information and some environmental parameters for each pixel. Some of these parameters like water vapor, view zenith angle, sun zenith angle etc. were used in my research as input parameters to perform the atmospheric correction. These parameters could be retrieved by using Matlab.

Table 3 MERIS spectral bands and applications

Band index	Band Centre (nm)	Band width (nm)	Application(s)
1	412.5	10	Yellow substance and detrital pigments
2	442.5	10	Chlorophyll absorption maximum
3	490	10	Chlorophyll and other pigments
4	510	10	Suspended sediment. Red tides
5	560	10	Chlorophyll absorption minimum
6	620	10	Suspended sediment
7	665	10	Chlorophyll absorption & fluorescence Reference
8	681.25	7.5	Chlorophyll fluorescence peak
9	708.75	10	Fluo. reference, atmosphere corrections
10	753.75	7.5	Vegetation. Cloud
11	760.625	3.75	O_2 R-branch absorption band
12	778.75	15	Atmosphere corrections
13	865	20	Vegetation. Water vapour reference

14	885	10	Atmosphere corrections
15	900	10	Water vapour. Land

2.3. Atmospheric correction

2.3.1. MODTRAN simulations

In this research, atmospheric correction (AC) of MERIS data was performed by using MODTRAN 5.2.1, based on the radiative transfer model. The input of MODTRAN file is a tape 5 text file and it contains several parameters to determine the real atmosphere condition in Table 4. The spectral region simulated was from 350 nm – 1000 nm with a 1nm step. We changed aerosol type, visibility and made totally 15 scenarios for the look-up table. For each scenario the MODTRAN interrogation technique was applied by using surface albedos of 0.0, 0.5 and 1.0. The output tape-7 file of MODTRAN quantified the TOA radiance for each simulated wavelength from 350nm to 1000nm. Then the tape 7 file was used as the input to compute four atmospheric parameters L_0, G_t, G_b, S by using the Eq. (2.3.4) and Eq. (2.3.5) in MATLAB. Then we computed these four atmospheric parameters (L_0, G_t, G_b, S) four the MERIS bands (total 15 bands) by using Eq. (2.3.8). Finally, we used Eq. (2.3.6) to derive water leaving reflectance R_{rs}.

Table 4 Input of MODTRAN parameters

Input parameters	values
Geographical-seasonal model	Mid-latitude summer
Concentration of CO_2 (ppm)	385.000
Water vapour (g/cm^2)	2.9
Ozone (DU)	320
Aerosol type	Rural, urban, marine
Visibility (km)	5, 10, 15, 20, 30, 40
Surface height (km)	0
Sensor height (km)	800
Relative azimuth angle (degree)	19
Solar zenith angle (degree)	30
View zenith angle(degree)	15
Albedo	0.00, 0.50, 1.00
Start, end wavelength, increment and band	350 - 1000 nm, 1.0, 1.0

2.3.2. Sensitivity analysis of MODTRAN input parameters

In the MERIS image, some of the retrieved parameters can be used as the input for MODTRAN. These input parameters are always spatially variable. However, we do not need to change each input value for each pixel to perform the atmospheric correction. It would need a lot of time and some of these input parameters do not influence the result a lot. It is better to use an average value for these parameters, if the varied parameters influence a little. Therefore, we should know how these input parameters influence the MODTRAN results in different input scenarios by using Matlab.

So, the sensitivity analysis for those parameters is necessary to see how the changes of these parameters influence the atmospheric correction results quantitatively.

The influence of the different MODTRAN input atmospheric parameters on changes in the radiance was analysed with a Matlab script. In the MODTRAN tp5 file, some parameters can be varied, such as aerosol type, visibility, solar zenith angle, view zenith angle etc. and the other parameters can be set as default if they do not influence the result a lot in my case. Here, four parameters were taken into consideration to analyse the sensitivity: visibility, view zenith angle, water vapour, ozone. Because firstly, visibility is the one of the most important parameters that we need to retrieve from the MODTRAN simulations. It is determined by the aerosol that is related to the quality of atmospheric correction directly. Secondly, view zenith angle, ozone and water vapour values changed a lot in different parts of MERIS image. Water vapour also influences the absorption of the path radiance directly. We should know how the changes of parameters influence the output results.

The sensitivity analysis equation as below:

$$dR = \frac{R(2) - R(1)}{R(2)}$$
$$dp = \frac{p(2) - P(1)}{p(2)}$$
$$Sp = \frac{dR}{dp} * 100 \qquad (2.3.1)$$

Here, *R* is the atmospheric path radiance;

P is different atmospheric parameters;

S is the sensitivity in percentage.

2.3.3. Simplified atmospheric modeling

For a uniform Lambertian surface and a homogeneous atmosphere, according to the four-stream radiative transfer theory , TOA radiance can be calculated by (Verhoef & Bach, 2003). This is illustrated by Fig. 4.

$$L^{TOA} = \frac{E_s^o cos_{\theta_s}}{\Pi}[\rho_{so} + \frac{(\tau_{ss}+\tau_{sd})r(\tau_{do}+\tau_{\infty})}{1-r\rho_{dd}}] \qquad (2.3.2)$$

Here, L^{TOA} is the total radiance at the TOA;

The ρ and τ symbols with double subscripts are reflectances and transmittances. The subscripts *s*, *d* and *o* indicate the direct solar flux, upward and downward diffuse, and the radiance to the observer, respectively.

θ_s is the solar zenith angle;

E_s^o is the extraterrestrial solar irradiance;

r is the surface reflectance.

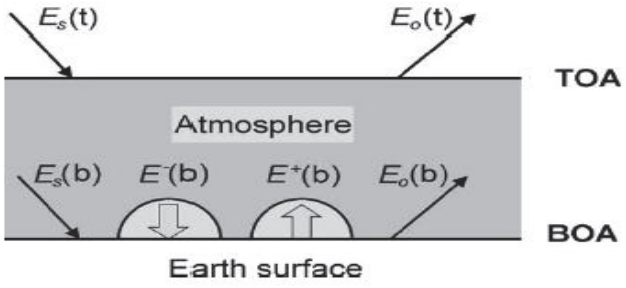

Figure 4 Four-stream radiation fluxes in optical modeling of the atmosphere

Eq. (2.3.2) can be simplified to:

$$L^{TOA} = L_0 + \frac{(Gt+Gb)*r}{1-r*S} \tag{2.3.3}$$

Here, L_0 is the atmosphere path radiance for zero surface reflectance;

G is the gain factor; G_t is the gain factor from target, G_b is gain factor from background;

r is target reflectance;

S is the spherical albedo of the atmosphere at ground level;

$L^{TOA}$is the TOA radiance.

Ignoring adjacency effects by assuming a uniform reflectance r, the following quantities are used for the atmospheric correction:

$$G = Gt + Gb = \frac{E_s^o \cos\theta_s}{\pi}(\tau_{ss} + \tau_{sd})(\tau_{do} + \tau_{oo});$$
$$S = \rho_{dd};$$
$$L_0 = \rho_{so}\frac{E_s^o \cos\theta_s}{\pi} \tag{2.3.4}$$

These parameters L_o, S, G can be derived from the outputs of the MODTRAN model by running the model 3 times. Running this model needs the atmospheric state and angular geometry parameters as inputs and sets the surface reflectance r as 0, 0.5, and 1, respectively. The corresponding outputs are called $LTOT_0$, $LTOT_{50}$, and $LTOT_{100}$. The atmospheric parameters are derived by the following equations(Shen, Verhoef, et al., 2010):

$$L_0 = LTOT_0;$$
$$S = \frac{\Delta_{100}-2\times\Delta_{50}}{\Delta_{100}-\Delta_{50}};$$
$$G = \Delta_{100} \times (1-S);$$
$$\Delta_{100} = LTOT_{100} - LTOT_O \ ;$$
$$\Delta_{50} = LTOT_{50} - LTOT_0 \tag{2.3.5}$$

The parameters L_0, S, G are spectral variables and dependent on inputs parameters of the MODTRAN model. Then look-up tables (LUTs) are generated that contain the L_0, S and G values in different bands and corresponding inputs parameters in each scenario to resolve the inversion problem of retrieving the remote sensing reflectance R_{rs} (Shen, Verhoef, et al., 2010):

$$r = \frac{L^{TOA} - L_0}{G + (L^{TOA} - L_0)S};$$
$$R_{rs} = \frac{r}{\Pi} \quad (2.3.6)$$

Here, r is the irradiance reflectance;

R_{rs} is the remote sensing reflectance.

Such process is called standard atmospheric correction. In my case, I also used the basic principle of MODTRAN to perform the atmospheric correction on MERIS images. Because of the spatially variable haze, the atmospheric correction actually should be performed pixel by pixel instead of the standard atmospheric correction. Here, the MERIS image was chosen from April 25 2008. In this case the atmosphere conditions could be considered homogeneous in my study, which has been validated in the previous research(Shen, Verhoef, et al., 2010). So, the standard atmospheric correction could be applied for this image processing.

2.3.4. Spectral response function (SRF)

The simulated spectral wavelength is from 350 nm to 1000 nm by using MODTRAN which increased 1nm each time. However, MERIS only has 15 bands from 400 nm – 900 nm. In order to compute the simulated MODTRAN runs for the MERIS bands, the spectral response functions of the MERIS bands should be used, which are shown in Fig. 5 and Fig. 6. The *X*-axis shows the wavelength scale; on the *Y*-axis the spectral response functions are shown. It can be used to define the corresponding atmospheric parameters for MERIS bands by using Eq. (2.3.7):

$$P_M(\lambda) = \frac{\sum(p(\lambda) * SRF(\lambda))}{\sum SRF(\lambda)} \quad (2.3.7)$$

where, $P_M(\lambda)$ is the atmospheric parameters computed for MERIS bands;

$p(\lambda)$ is one of the three atmospheric parameter (L_0, S, G) values at MODTRAN wavelengths;

$SPF(\lambda)$ is the weight of the spectral response function for the MERIS band.

Here, these three atmospheric parameters (L_0, S, G) for each MERIS band can be simplified by computing the average of the corresponding MODTRAN simulated results which are in each MERIS band range in Eq. (2.3.8).

$$P_M(\lambda) = \frac{\sum(p_1(\lambda) + \cdots + p_n(\lambda))}{n} \quad (2.3.8)$$

where, $P_M(\lambda)$is the atmospheric parameters for each MERIS bands;

$p(\lambda)$ is the three atmospheric parameters (L_0, S, G) values at MODTRAN wavelengths;

n is the number of the MERIS bands.

For these three parameters, 15 values which are spectrally varied with MERIS bands can be got. Afterwards, the water leaving reflectance therefore could be derived for each MERIS band by using these three atmospheric parameters according to Eq. (2.3.6).

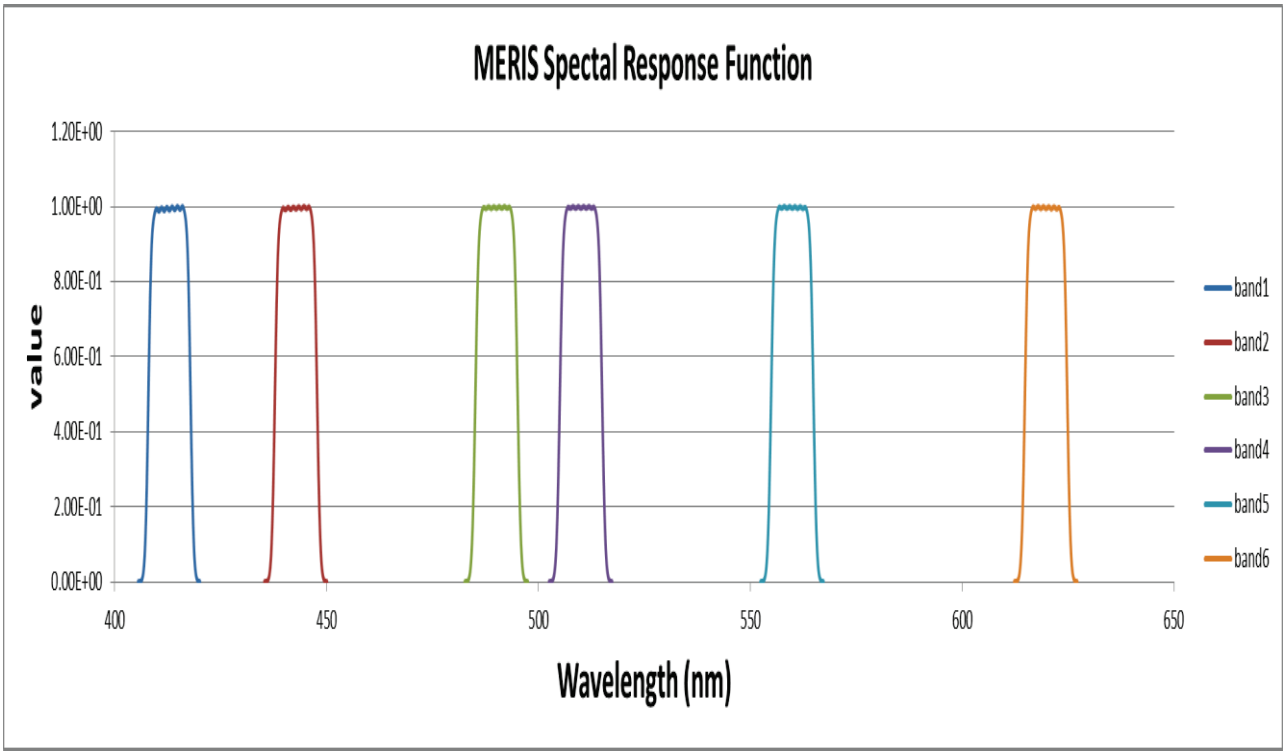

Figure 5 MERIS spectral response functions (band 1-6)

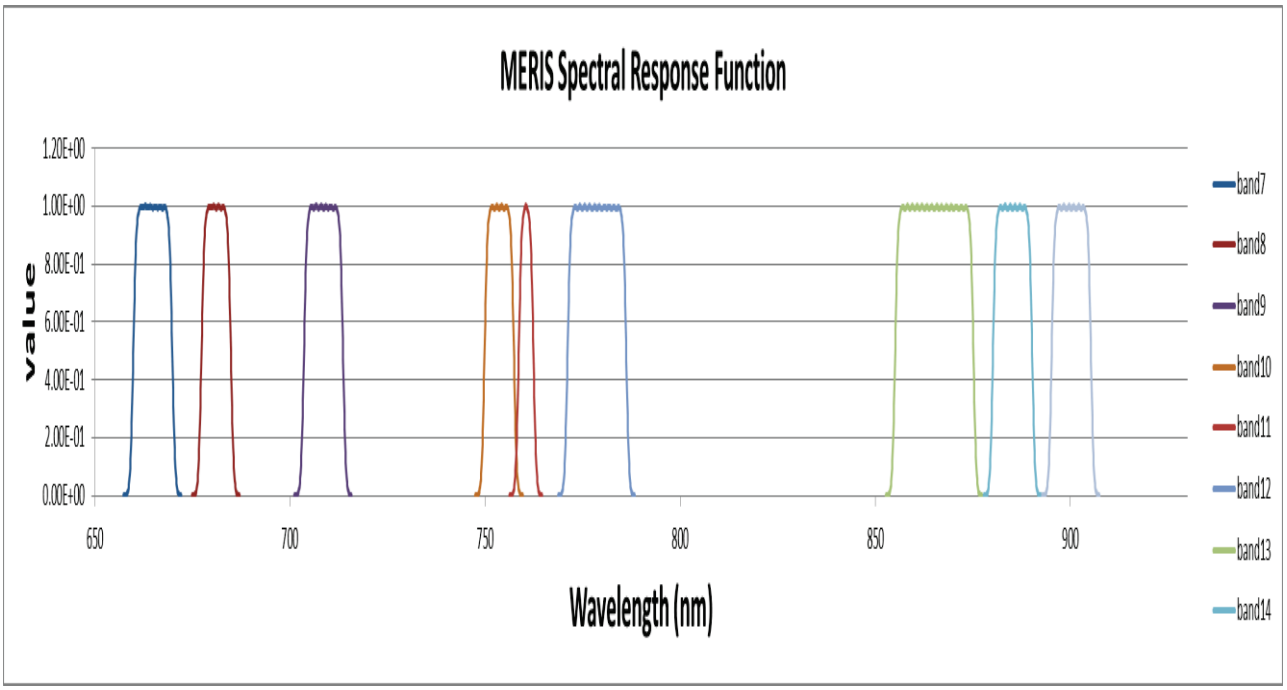

Figure 6 MERIS spectral response functions (band 7- 15)

2.3.5. C2R processor

The Case-2 regional processor consists of the atmospheric correction procedure and water quality algorithms procedures. The atmospheric correction is based on the radiative transfer model using neutral network (NN) algorithms. MERIS has 4 bands which are used to perform the atmospheric correction. However, only using four bands could lead to partly mistaken in very high absorption or scattering area due to the bands saturation. So in the C2R processor, 12 bands (412, 442, 490, 520, 560, 620, 665, 681, 709, 756, 778, and 865 nm) are used for atmospheric correction. The atmospheric correction scheme is illustrated in Fig. 7 as below:

(1) - (4) are the input values taken from the MERIS L1 product pixel by pixel except for the solar flux. The input variables are determined from the training and test data set for creating the atmospheric correction neutral network NN.

(5) is used for computing the top of standard atmosphere (TOSA) radiance reflectance (*RL*_tosa) by using the deviation of the atmospheric pressure and ozone concentration from the standard values, i.e. 1013 hPa and 350 Dobson units (DU).

(6) is the module for the correction of the influence of water vapour on band 9 (708 nm), it was performed by implementing in the IPF ground processor.

(7) Optional procedures for correcting or reducing the camera boundary problem (smile correction) and for considering the polarization in the atmosphere

(8) The atmospheric correction neural network NN, which takes the influence of aerosols, thin cirrus clouds, sun and sky glint and the water leaving radiance into account.

(9) – (12) output of the NN: (9) path radiance reflectance, i.e. radiance entering the sensor from all sources above the water surface, (10) transmittance, (11) water leaving radiance reflectance, (12) aerosol optical thickness for 4 wavelengths, (13) aerosol Angstrom coefficient alpha computed from the aerosol optical thicknesses at 443 and 865 nm.(Doerffer & Schiller, 2008)

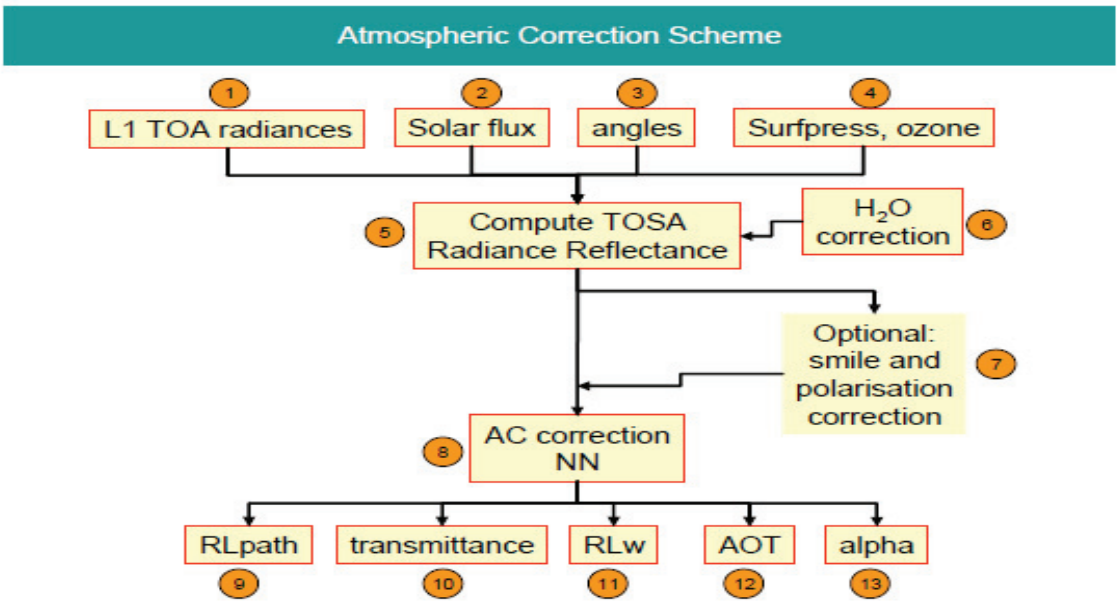

Figure 7 Algorithm of the atmospheric correction in the case-2 regional processor

In my case, the atmospheric correction and the smile correction were processed by using the C2R processor plug-in in BEAM 4.9 version software. The input data is MERIS L1B FR image on April 25 2008. The corresponding output is MERIS L2 product contains water leaving reflectance for 12 bands (412, 442, 490, 520, 560, 620, 665, 681, 709, 756, 778, and 865 nm), water leaving path reflectance, aerosol optical thickness for four bands(443, 550, 778, 865nm) and water quality parameters.

2.3.6. Comparing reflectances between two atmospheric correction models

When comparing two atmospherically corrected reflectances, four Pins (Pin1, 2, 5, 6) shown in Fig. 22 with different levels of SSC were chosen. According to Fig. 10, these chosen pins are at least in that ranges. Then, we roughly compared the water leaving reflectances by the MODTRAN model and the C2RP with the water leaving reflectance from the previous research(Shen, Suhyb Salama, et al., 2010) . In that research, the reflectance was estimated in a tank experiment in Fig. 8. However, in a real environment, the reflectance is not always like those from the experiment. So it is just a rough comparison to show which atmospheric correction is better in my case. More comparison between simulated reflectance by the Duntley model and the retrieved reflectance by two atmospheric correction models are shown in section 2.4.

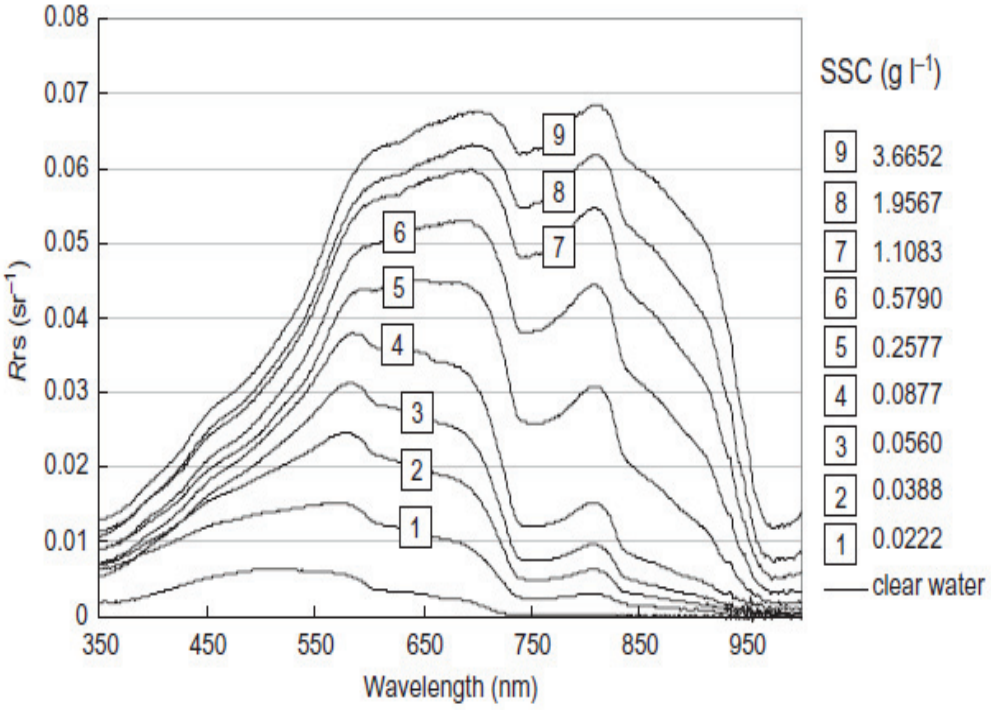

Figure 8 Spectral shapes of Rrs at different levels of SSC in the tank experiment for the Yangtze River estuary (Shen, Suhyb Salama, et al., 2010)

2.4. SSC retrieval algorithm

Focusing on our target (water), after processing the atmospheric correction, we can also link the radiance at the bottom of atmosphere with water optical properties using equations, based on the radiative transfer

inside the water. The Duntley water model was used in my research to link the water leaving reflectance with optical properties in water.

In Fig. 9, a detail flow chart about SSC retrieval algorithm (purple part in Fig. 3) in my research is shown below.

In Fig. 9, the algorithm is about how to generate the SSC map from the water leaving reflectance that is based on the MODTRAN atmospheric correction model. Since the SSC map based on C2RP was also generated by using the same algorithm in Fig. 9. Here, we do not mention it again.

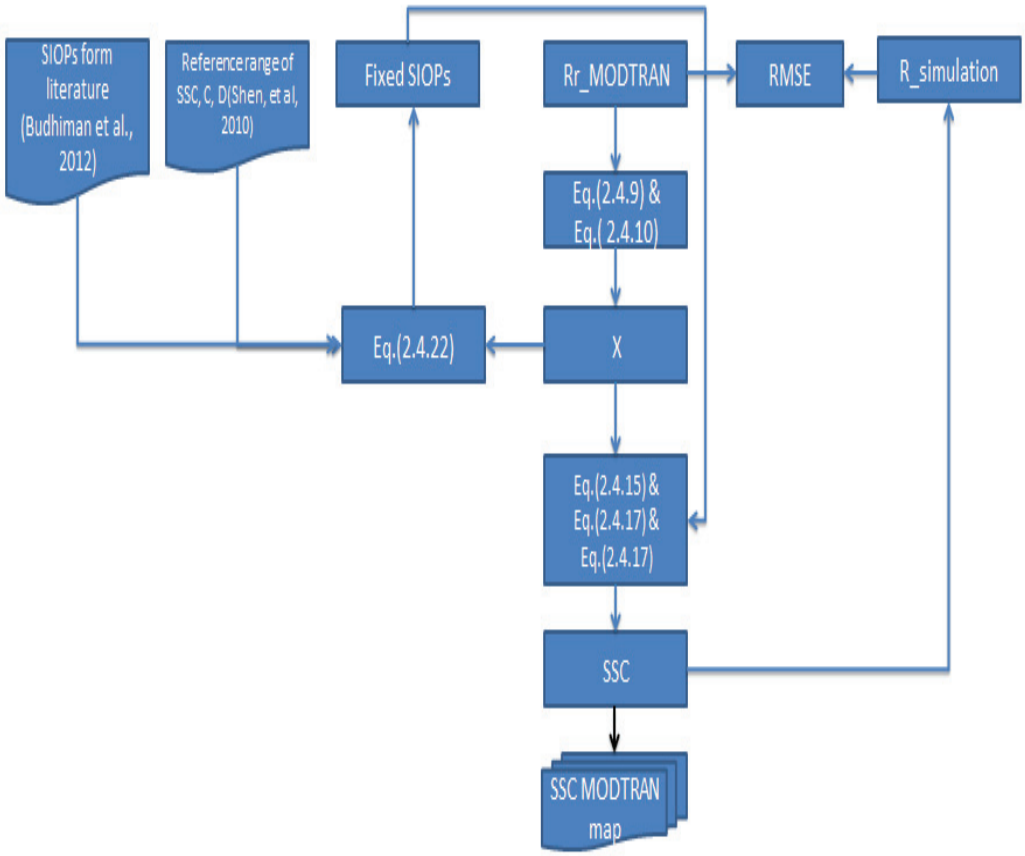

Figure 9 The flow chart of the SSC retrieval algrithm

2.4.1. The Duntley equations and Lee equations

The Duntley equations (Duntley, 1942) are similar to K-M theory in respect of assuming two hemispherical diffuse streams, one upward and one downward. However, the Duntley equations are a two-stream theory that adds the direct radiation from the sun to the system of differential equations. Especially, under sunny conditions, it is better to consider the effects of direct solar radiation.

Radiative transfer inside the water column can be described by the Duntley equations (Duntley, 1942) as follows:

$$\frac{dE_s}{d_Z} = KE_s$$
$$\frac{dE^-}{d_Z} = -s'E_s + \alpha E^- - \sigma E^+$$
$$\frac{dE^+}{d_Z} = sE_s + \sigma E^- - \alpha E^+ \quad (2.4.1)$$

where E_s is the direct solar flux, and E^- and E^+ are the diffuse downward and upward fluxes, respectively, and Z is supposed to increase in upward direction and to be zero at the top, so that it is negative under water.

The extinction coefficient for direct sunlight is K. It is related to the absorption coefficient a and the total scattering coefficient b by:

$$k = \frac{a+b}{\cos\theta_s'} \quad (2.4.2)$$

The scattering coefficients for direct sunlight are called s for backscattering and s' for forward scattering and are given by:

$$s = \frac{b_b}{cos\,\theta_s'} \quad s' = \frac{b_f}{cos\,\theta_s'}$$
$$b = b_f + b_b$$
$$\mu_w = cos\,\theta_s' \quad (2.4.3)$$

Here, b_b is the backscattering coefficient;
b_f is the forward scatter coefficient;
θ_s' is the under-water solar zenith angle.

The coefficients α and β also occur in the Kubelka-Munk theory, and are known as the attenuation coefficient and the backscatter coefficient for diffuse radiation, respectively. Important relationships are:

$$\beta = 2b_b \quad \alpha = 2(a + b_b) \quad m = \sqrt{\alpha^2 - \beta^2} \quad (2.4.4)$$

r_∞ is the so-called infinite reflectance of the medium (Kubelka & Munk, 1931):

$$r_\infty = \frac{\frac{b_b}{a}}{1+\frac{b_b}{a}+\sqrt{1+2\frac{b_b}{a}}} = \frac{x}{1+x+\sqrt{1+2x}} \quad (2.4.5)$$

Here, x is the ratio of backscattering coefficient and absorption coefficient;
b_b is the backscattering coefficient;
a is the absorption coefficient.

When we add solar radiance, we can use the underwater irradiance reflectance for sunlight r_{sd}^{∞} as a basis for estimation of water optical properties:

$$r_{sd}^{\infty} = \frac{s+s'r_{\infty}}{k+m} \quad (2.4.6)$$

It can be linked to the underwater reflectance r_{rs} by the following equation (Lee et al., 1998):

$$r_{sd}^{\infty} = Qr_{rs} \quad (2.4.7)$$

Here, Q is the ratio of subsurface upwelling irradiance to upwelling radiance; Q =3.25
It can be derived that, the forward equation for r_{rs} is given by:

$$r_{rs} = \frac{\sqrt{1+2x}-1}{Q(\sqrt{1+2x}+2\mu_w)} \quad (2.4.8)$$
$$\mu_w = \cos\theta_s'$$

where θ_s' is the under-water solar zenith angle. If the above-water solar zenith angle is θ_s, then the under-water solar zenith angle is found with Snell's law from, $\theta_s' = arcsin(\ sin\theta_s/n_w)$, where n_w is the refraction index of water, which here is equal to 1.33.
The inverted equation is given by:

$$x = \frac{Qr_{rs}(1+2\mu_w)[1+Qr_{rs}(\mu_w-0.5)]}{(1-Qr_{rs})^2} \quad (2.4.9)$$

R_{rs} is the remote sensing reflectance measured above water. This quantity can be converted into r_{rs}, by the following empirical formula(Craig et al., 2006) :

$$r_{rs} = \frac{R_{rs}}{0.52+1.7R_{rs}} \quad (2.4.10)$$

2.4.2. The matrix inversion method

The Duntley equations characterize the relation between underwater reflectance and water optical properties. But they lack a direct link to the SSC.
The elegant matrix inversion method (MIM) can be applied to link the water optical properties and SSC, which can give a direct answer of SSC and thus is very fast.
The x value is the ratio of the bulk backscattering coefficient and the absorption coefficient of the water. Here, we assume the SIOPs (specific inherent optical properties) of the water components, namely suspended sediment, chlorophyll, CDOM and pure water in water. So:

$$x(\lambda) = \frac{S\times b_S(\lambda)\times B + b_w(\lambda)}{a_w(\lambda)+S\times a_S(\lambda)+C\times a_c(\lambda)+D\times a_D(\lambda)} \quad (2.4.11)$$

$b_S(\lambda)$ is the specific backscattering coefficient of the suspended of sediment;
$b_W(\lambda)$, $a_W(\lambda)$ are the specific backscattering and absorption of water.
$a_S(\lambda)$, $a_C(\lambda)$, $a_D(\lambda)$ are the specific absorption coefficients of suspended sediment, chlorophyll, and colored dissolved organic matter, respectively;
B is the fraction of backscattering;
S is the concentration of suspended sediment,

C is the concentration of chlorophyll;
D is the concentration of colored dissolved organic matter.
Then, for each spectral band, Eq. (2.4.11) can be rewritten as the linear equation:

$$S * (xa_s(\lambda) - b_s(\lambda) * B) + C * x(\lambda)a_c(\lambda) + D * x(\lambda)a_D(\lambda) = b_w(\lambda) - x(\lambda)a_w(\lambda) \quad (2.4.12)$$

In the case of *n* spectral bands one obtains *n* equations of this kind, from which one can solve *S*, *C* and *D* if three or more spectral bands are used. For *n* bands the set of equations can be written in matrix-vector form as

$$\begin{pmatrix} x_1a_{s,1} - b_{s,1} & x_1a_{c,1} & x_1a_{d,1} \\ \vdots & \vdots & \vdots \\ x_na_{s,n} - b_{s,n} & x_na_{c,n} & x_na_{d,n} \end{pmatrix} \begin{pmatrix} S \\ C \\ D \end{pmatrix} = \begin{pmatrix} b_{w,1} - x_1a_{w,1} \\ \vdots \\ b_{w,n} - x_na_{w,n} \end{pmatrix} \quad (2.4.13)$$

where the second subscript indicates the spectral band number. This equation can be written in shorthand notation as **Mc** = **w**, where **M** is the left-hand matrix, **c** is the vector containing the concentrations *S*, *C* and *D*, and **w** is the right-hand vector. In the case of 3 spectral bands one can find the solution directly by matrix inversion from $\mathbf{c} = \mathbf{M}^{-1}\ \mathbf{w}$. However, this solution might be sensitive to noise, and for more stability it is therefore better to use more than 3 spectral bands. In that case one can find the least squared error solution by using the transposed of matrix **M**, $\mathbf{M}^{\mathrm{T}}$, and writing

$\mathbf{M}^{\mathrm{T}}\mathbf{M}\mathbf{c} = \mathbf{M}^{\mathrm{T}}\mathbf{w}$, which gives the solution as $\mathbf{c} = (\mathbf{M}^{\mathrm{T}}\mathbf{M})^{-1}\mathbf{M}^{\mathrm{T}}\mathbf{w}$. (2.4.14)

Here, in my case, *C* and *D* values can be estimated which will be discussed in section 2.4.3. Therefore, only the *S* value is unknown and then Eq. (2.4.12) can be rewritten as:

$$S(\lambda) = \frac{(a_w(\lambda)+a_c(\lambda)*C+a_D(\lambda)*D)*x(\lambda)-b_w(\lambda)}{b_s(\lambda)*B-a_s(\lambda)*x(\lambda)} \quad (2.4.15)$$

$$M(\lambda) = (a_w(\lambda) + a_c(\lambda) * C + a_D(\lambda) * D) * x(\lambda) - b_w(\lambda)$$

$$N(\lambda) = b_s(\lambda) * B - a_s(\lambda) * x(\lambda) \quad (2.4.16)$$

Here, $M(\lambda)$ and $N(\lambda)$ values changed in each band, so that the *S* value also varied with the spectral bands, so S value in each pixel can be determined by using Eq. (2.4.17):

$$S_{mean} = \frac{\sum M(\lambda)}{\sum N(\lambda)} \quad (2.4.17)$$

Summarized, from R_{rs} in a number of spectral bands one can invert the Duntley model, which gives the *x* values in these spectral bands. Next, the matrix inversion method can be applied to derive the concentrations *S* from the *x* values, *C*, *D* concentration and the assumed SIOPs.
When using the MIM to retrieve the SSC, the spectral bands we used should meet the following requirements:

1) The curves (*X*-axis is concentration, *Y*-axis is reflectance) of these bands cannot overlap with each other too much. They should be independent, not influence each other.
2) The bands that we chose should be sensitive to the concentration. It means the reflectance values should vary with the suspended sediment concentration.
3) We use the bands with maximum sensitivity.

Hence, it is better to use multispectral or hyperspectral bands to retrieve different concentration range to ensure maximum sensitivity, so as to get a higher accuracy of retrieval.

2.4.3. Determining simulated spectral inherent optical properties (SIOPs)

SIOPs are optical properties related to the individual scattering and absorption of water constituents. In my case, suspended sediment, chlorophyll, CDOM and pure water in water are under consideration.
First, all SIOPs values were used from the literature(Budhiman et al., 2012) directly. So, according to the Eq. (2.4.11), the values of the absorption coefficient of water molecules a_W, the values of the backscattering coefficient of water molecules b_W, the values of the Chl-a absorption coefficient a_C, the values of the absorption of CDOM a_{CDOM}, the values of the absorption coefficient a_S and the values of the backscattering coefficient of sediment b_S.
Here, the Chl-a absorption coefficient a_C was approximated using an empirical model (Lee et al., 1998, 1999):

$$a_{chl}(\lambda) = (c_0(\lambda) + c_1(\lambda)\, ln\, a_{chl}(440)) \times a_{chl}(440) \quad (2.4.18)$$

where, C_0 and C_1 are independent spectrally variable constants.
$a_{chl}(440)$ is the specific absorption coefficient at wavelength of 440 nm.

The absorption of CDOM decreases with the increase of wavelength and was approximated using the exponential equation(Bricaud et al., 1981):

$$a_{CDOM}(\lambda) = a_{CDOM}(440)\exp(-S_{CDOM}(\lambda - 440)) \quad (2.4.19)$$

where, s is the spectral coefficient;
a_{CDOM} is the specific coefficient in 440nm.

The backscattering coefficient of TSM can be parameterized by (Kopelevich, 1983):

$$b_S(\lambda) = b_S(550)(\frac{550}{\lambda})^{\alpha} \quad (2.4.20)$$

where, a is the spectral shape exponent, and $b_s(550)$ is the backscattering coefficient of TSM at the reference wavelength of 550 nm.

The absorption coefficient of the sediment concentration a_S should fit the Eq. (2.4.21) (Lee et al., 1999)below:

$$a_S(\lambda) = a_S(440)\exp(-S_S(\lambda - 440) \quad (2.4.21)$$

where, s_S is the spectral coefficient;

a_S is the specific coefficient in 440nm.

However, in my case, this SIOPs values cannot be used directly. Because the simulated reflectance curves by Duntley always show disagreement with the retrieved curves by the MODTRAN atmospheric correction model, which are shown in section 3.4.1.

Therefore, a new group of SIOPs values were estimated for my study area. We assumed the new group of SIOPs can fit the retrieved reflectance by MODTRAN with the simulated curves by the Duntley model better.

$a_W(\lambda)$, $b_w(\lambda)$, $a_C(\lambda)$, $a_D(\lambda)$ and $b_S(\lambda)$ values were also chosen from literature and just assumed a new group of $a_S(\lambda)$ values. So, $a_W(\lambda)$, $b_w(\lambda)$, $a_C(\lambda)$, $a_D(\lambda)$, $b_S(\lambda)$, *S, C, D and* $x(\lambda)$ values can be used to express $a_S(\lambda)$, then Eq. (2.4.11) can be rewritten into:

$$a_S(\lambda) = \frac{B*b_B(\lambda)*S - D*a_D(\lambda)*x + b_w(\lambda) - x*a_W(\lambda)}{x(\lambda)*S} \quad (2.4.22)$$

Here, $a_W(\lambda)$, $b_w(\lambda)$, $a_C(\lambda)$, $a_D(\lambda)$, $b_S(\lambda)$ were chosen from the literature(Budhiman et al., 2012);

C and *D* were chosen from previous research(Shen, Zhou, et al., 2010);

$x(\lambda)$ values were retreived from the MODTRAN reflectance using Eq. (2.4.9) and Eq. (2.4.10).

On 25 April 2008, CHL-a concentration can be estimated from Fig. 11. In Fig. 11, the CHL-a concentration was ranging from 0.2 to 3.5 mg/m^3, which is not high. The study area can be divided into two parts like Fig. 10. A is turbid water and B is relative clean water. In area A (121°30'E- 122°30'E), CHL-a concentration is below 1.0 mg/m^3. In area B (122°30'E- 123°E), CHL-a concentration is between 1.0 to 3.5 mg/ m^3. When comparing with the SSC, such a low CHL-a concentration has much less influence on the water leaving reflectance due to the high SSC value which has a dominant influence on the result. Therefore one average value for area A and one average value for area B were determined for the CHL-a concentration in Table 5.

CDOM values was determined in a range of 0.06 - 0.47 for the Yangtze River estuary that were chosen from the literature. Clean water has lower CDOM concentration than the turbid water in my study area. Similarly, one average value for turbid water (area A) and one value for clean water (area B) were determined in Table 5.

X values were retrieved from water leaving reflectance by the Duntley inversion water model using Eq. (2.4.9) and Eq. (2.9.10). The *S* value was simulated in the range according to Fig. 10.

We assumed that a_S values are different in turbid water and relative clean water. Therefore, two pixels were chosen here. One is from very a high sediment concentration area, the other pixel was chosen from clean water with low sediment concentration. These two pixels were used to estimate two groups of a_S values for turbid water and clean water, respectively. We assumed that these two groups of a_S can fit the simulated Duntley curves with the retrieved curves by the MODTRAN model better.

Table 5 CHL-a and CDOM concentration used in this study

Location	CHL-a(mg/m^3)	$a_g(440)/m-1$
Area A	1	0.3
Area B	3	0.15

When simulating a_S values, in my case, the retrieved reflectance values in band 1, band 11 and band 15 always showed wrong values. It may lead negative or too high a_S values for those bands.
Due to the new simulated a_S values should also fit the exponential function Eq. (2.4.21) (Lee et al., 1999). Thus, a_S values from the other 12 bands (without band 1, 11 and 15) according to Eq. (2.4.21) were used to invert a best fit S value (spectral coefficient) by program code. Then the S value and these 12 a_S values were used in Eq. (2.4.21) again to compute a_S values for those three bands (band 1, band 11 and band 15), in order to generate a fixed group of a_S values for each MERIS band. By using this method, two groups of a_S values were assumed for both turbid water and clean water.

2.5. Evaluation strategy

After having retrieved SSC values from the model in this research, it is necessary to evaluate the quality of the model by using four methods below:

2.5.1. Absolute RMSE

The absolute RMSE was calculated to compare the retrieved water leaving reflectance by the MODTRAN model with the simulated water leaving reflectance by the Duntley forward model:

$$Absolute\ RMSE = \sqrt{\frac{\sum_{i=1}^{n}(r_{Mi} - r_{si})^2}{n}}$$

where, r_s is the simulated reflectance which were generated by the retrieved SSC value by the Duntley model;
r_M is the retrieved reflectance by the MODTRAN atmospheric correction model;
n is the total band numbers. (2.5.1)

2.5.2. Relative RMSE

The relative RMSE next was computed to compare the retrieved water leaving reflectance by the MODTRAN model with the simulated water leaving reflectance by the Duntley forward model:

$$Relative\ RMSE = \sqrt{\frac{\sum_{i=1}^{n}(\frac{r_{Mi} - r_{si}}{r_{Mi}})^2}{n}}$$

where, r_s is the simulated reflectance which were generated by the retrieved SSC value by the Duntley model;
r_M is the retrieved reflectance by the MODTRAN atmospheric correction model;

n is the total band numbers. (2.5.2)

2.5.3. The linear regression

After having generated two SSC products by using the Duntley water model based on different atmospheric correction models (the MODTRAN model and the C2R processor), it is necessary for us to compare them approximately to show the disagreement and agreement. Further, 16 pins were randomly chosen shown in Fig. 22 to compare them using the linear regression. Here, log (SSC) from C2RP was plotted on the *X*-axis and log (SSC) from MODTRAN was plotted on the *Y*- axis.

2.5.4. Comparison with reference SSC products

Reference SSC and CHL-a data were chosen from the previous research that retrieved from a developed algorithm by using MERIS L1B images on April 25 2008 (Shen, Verhoef, et al., 2010; Shen, Zhou, et al., 2010). SSC is retrieved by the atmospheric correction MODTRAN model and the SERT water model shown in Fig. 10. In this figure, SSC can be divided into area A and B. Area A is turbid water and SSC ranged from 100 mg/L to more than 1000 mg/L. Area B is clean water and SSC is relatively low, below 100 mg/L. In Fig. 11, CHL-a concentration is retrieved by using the SCI algorithm which ranged from 0.27 mg/m^3 to 3.5 mg/m^3.Area A is below 1 mg/m^3 and area B ranged between 1- 3.5 mg/m^3.
In my research, when estimating simulated Duntley reflectance, the reference SSC and CHL concentration can be taken into consideration. A range of SSC and CHL-a concentration from the reference products were chosen to simulate Dunley reflectance and compared it with the results after atmospheric correction. Afterwards, because we do not have the exact SSC values from the reference SSC product (Shen, Verhoef, et al., 2010), the SSC products in my research could be compared roughly with the reference one to show the agreement and disagreement.

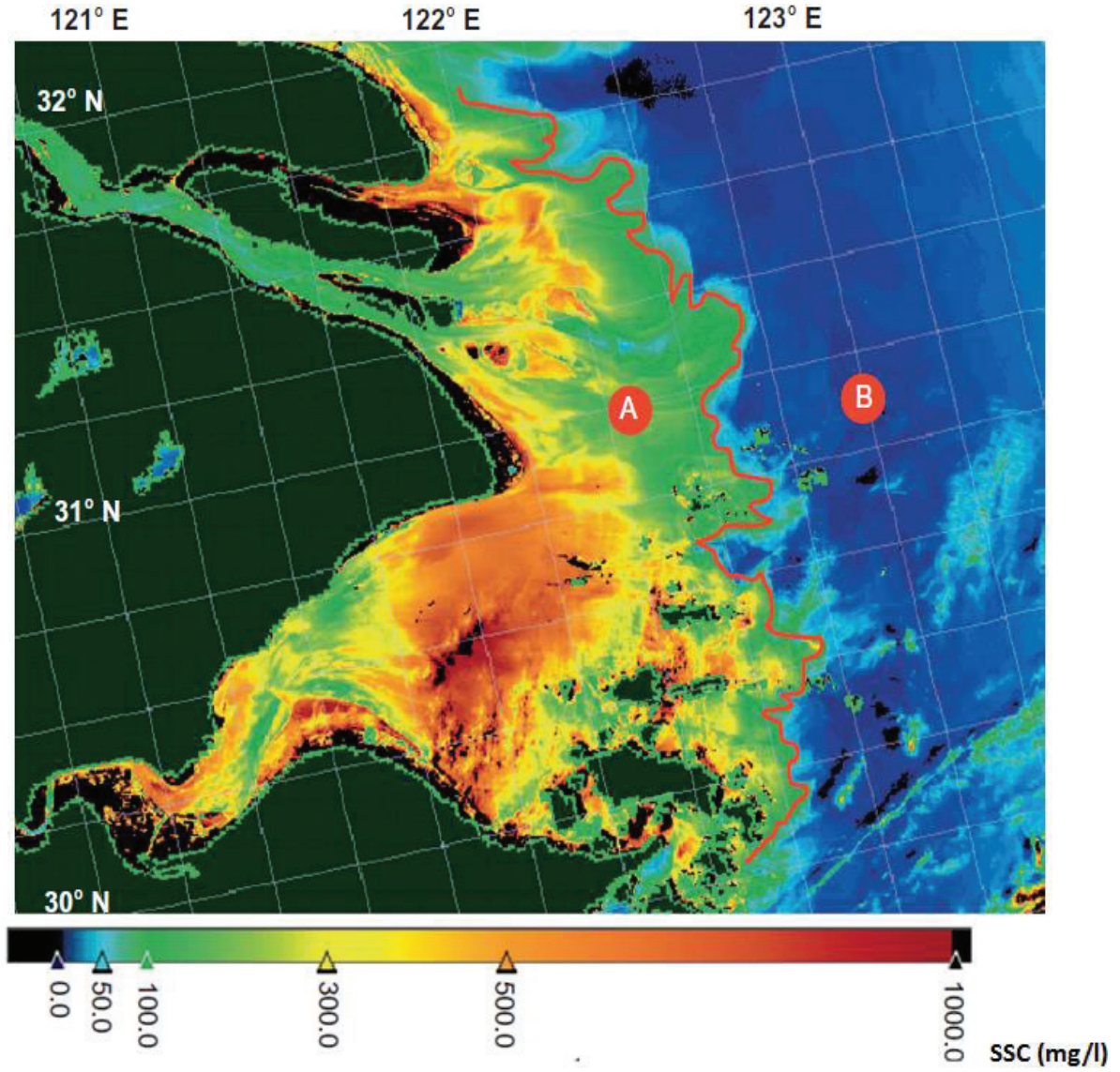

Figure 10 Sketch map of optically separated waters in the Yangtze Estuary. The turbidity front dividing line (red line) optically separates the waters into the sediment-dominated waters ('A' zone) and clean water ('B' zone). The SSC product is derived by using SERT model from the MERIS FR image on 25 April 2008. (Shen, Zhou, et al., 2010)

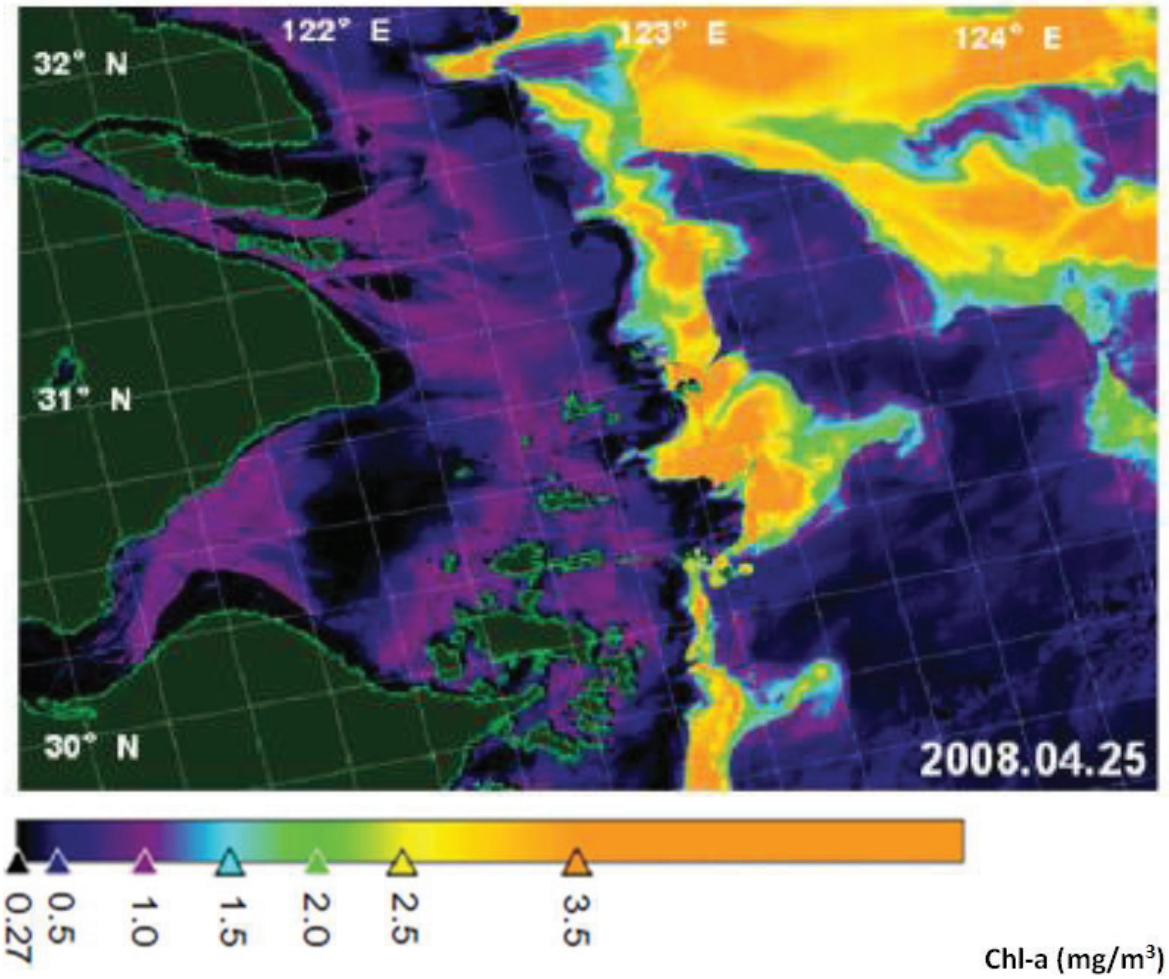

Figure 11 Chlorophyll-a concentration retrieved by the SCI algorithm from the MERIS FR image on 25 April (Shen, Zhou, et al., 2010)

3. RESULTS AND DISCUSSION

3.1. MODIS imagery results

3.1.1. MODIS spectral bands

In total 8 images from MODIS Aqua and Terra were chosen in my case. The images show that in some of these bands (8-19), the signals for sediment retrieval are saturated due to the sun glint and high sediment loads.

Fig. 12 is an example to show the saturation from MODIS Terra images on July 29 2007. There are three bands (8, 10, and 13) shown below. We can easily see a little, large and most of saturation in band 8, band 10 and band 13. Then one pixel in my study was randomly chosen to analyse the spectral profile of these bands (8-19) for the same image (July 29 2007). The result is shown in Fig. 13 and it turned out that most of the bands signal (8-19) are saturated (getting the maximum value of 4095).

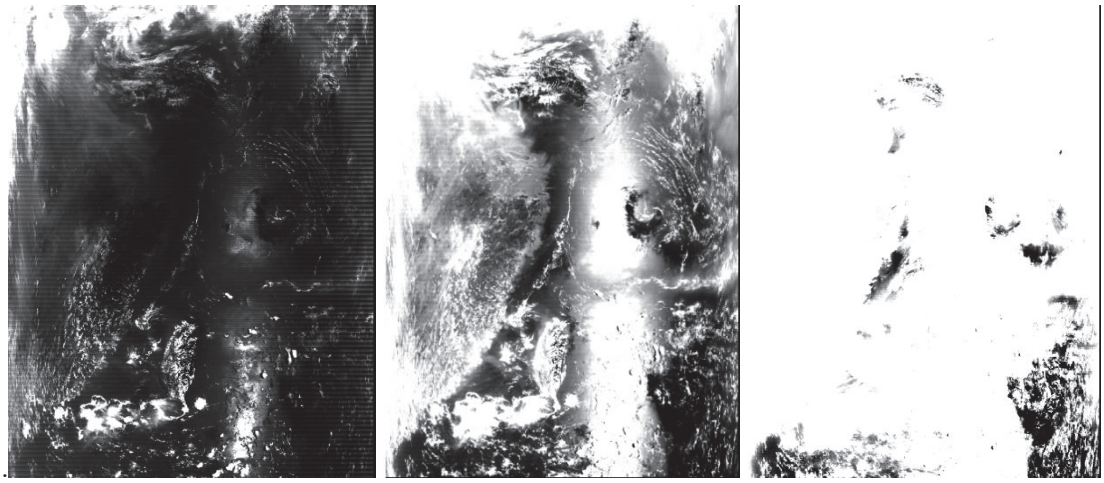

Figure 12 MODIS bands 8, 10 and 13 on July 29 2007

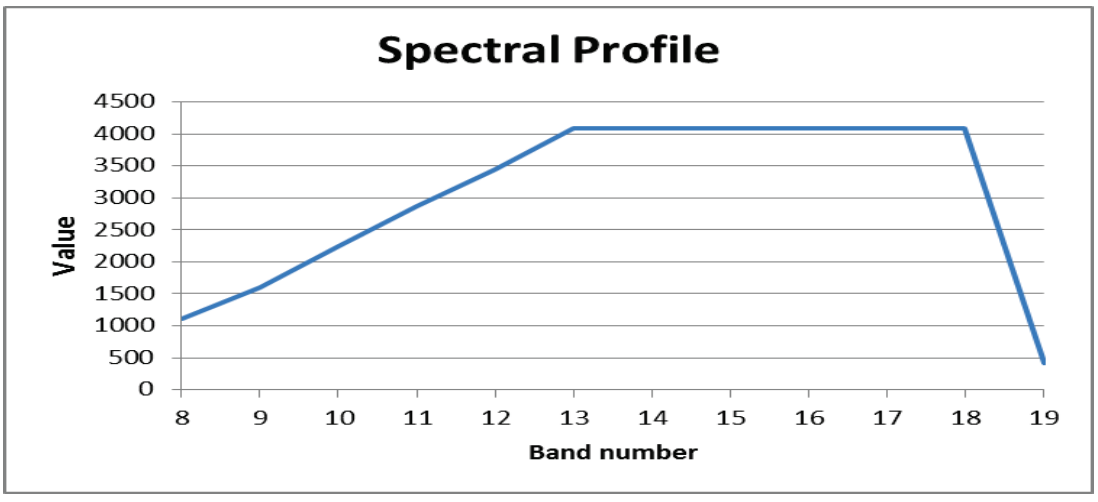

Figure 13 Analysis of Spectral profile result

3.1.2. Saturation analysis

Due to the band signal saturation shown in Fig. 13, the pixel values will not change any more. So these pixel values cannot be used to retrieve SSC. Then, a spectral calculation for each chosen MODIS image was performed using ENVI software to qualitatively analyse how many bands are saturated in each image and which parts are saturated in the image. In the spectral calculation, in each band, if the values are saturated, we set these values as 0. The other values are set as 1. Then a new map with values 0 to 12 could be generated. The value means how many bands are not saturated in each image. The results are shown in Fig. 14. In Figure 14, the green circle is my study area.

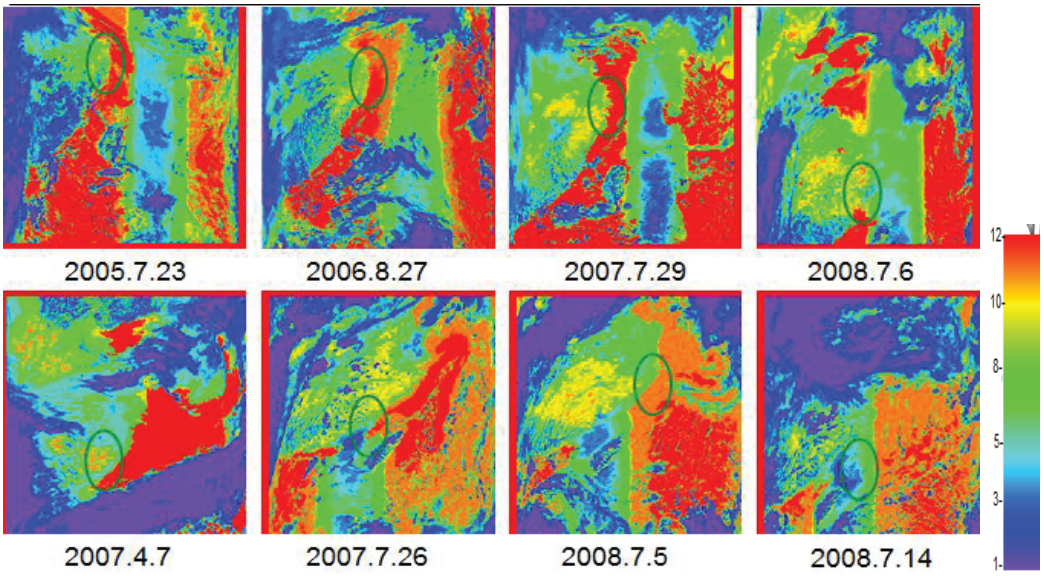

Figure 14 MODIS bands analysis results

The more red color means that more bands can be used and more blue color means fewer bands can be used. From the results (Fig.14), it is shown that MODIS images are just not suitable for my study. Because only a few bands can be used, our work is made more difficult. If my study is in the red part, then we can continue to use MODIS images.

3.2. MERIS imagery results

MERIS level 1b images turned out to be more suitable in my research. The scenes are from bands 2, 6 and 15 as an example on April 25 2008 in Fig. 15. It is quite clear to distinguish my study area unlike in the MODIS images.

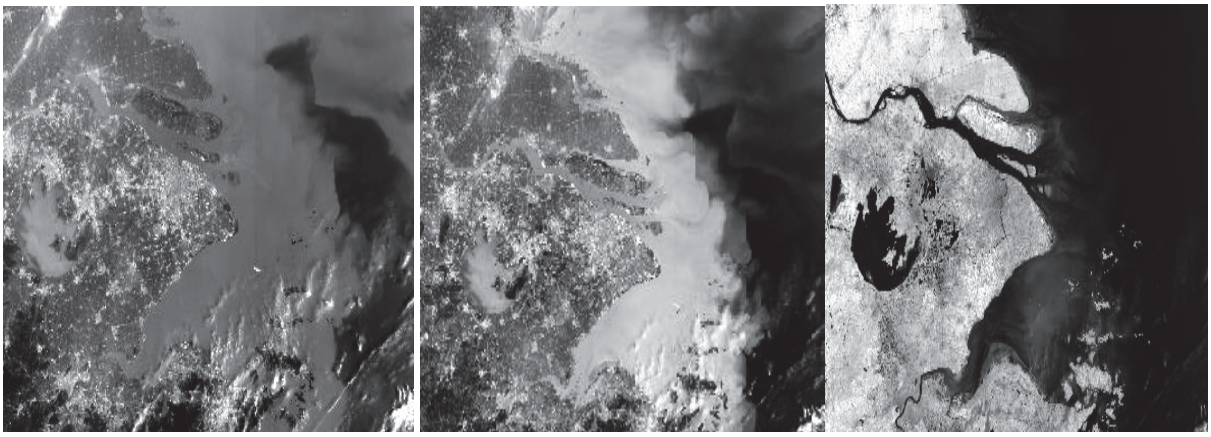

Figure 15 MERIS L1b images bands2, 6 and 15

Some of the environmental parameters retrieved from the MERIS image in my study area are shown in Fig. 16 by using Matlab. These parameters are also the input of MODTRAN parameters shown in Table 4. The results shown that relative humidity changed from 50 - 70, view zenith varied from 5 - 20, ozone concentration changed from 300 - 340 and sun zenith change from 28.5 to 30.5 in different parts of study area. However, it is better to use an average value for these parameters instead of changing each input value for each pixel to perform the atmospheric correction. So the sensitivity analysis is shown in section 3.3.3.

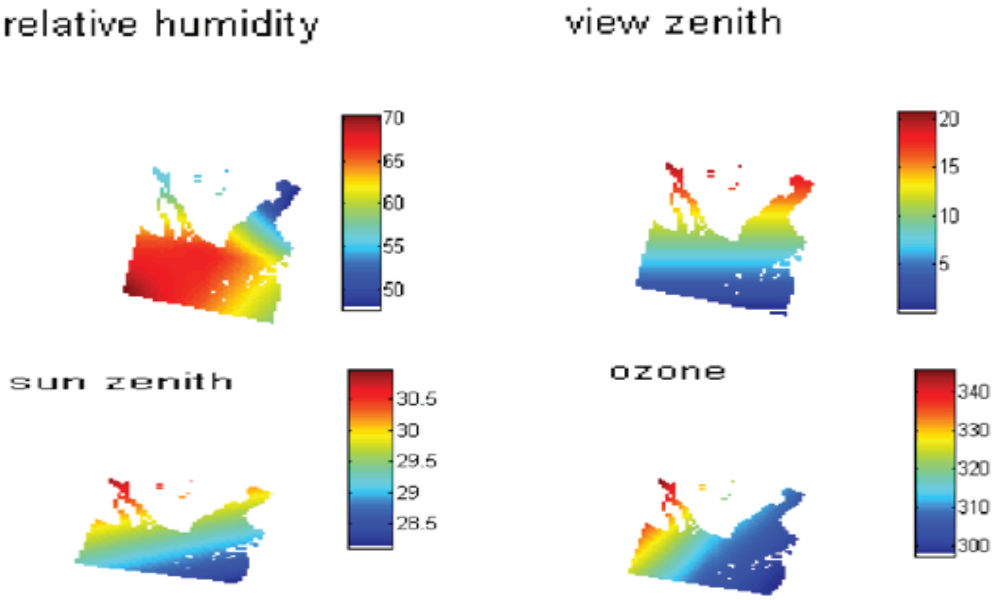

Figure 16 Some of the retrieved parameters from MERIS image on 25 April 2008

3.3. Atmospheric correction results

3.3.1. MODTRAN simulation results

Atmospheric correction from MODTRAN required retrieving atmospheric parameters like aerosol optical thickness (AOT) for retrieval the reflectance from radiance from MERIS level 1b images. The

MODTRAN simulated results can be used to compute four atmospheric parameters for each wavelength in MATLAB script are shown in Fig. 17. In Fig. 17 (a), L_0, S, G_t, G_b are shown in different colors. G_t values are larger than G_b and L_0. The S values are very small and close to 0. In order to see S values clearly, S simulation values were plotted again in Fig. 17 (b).

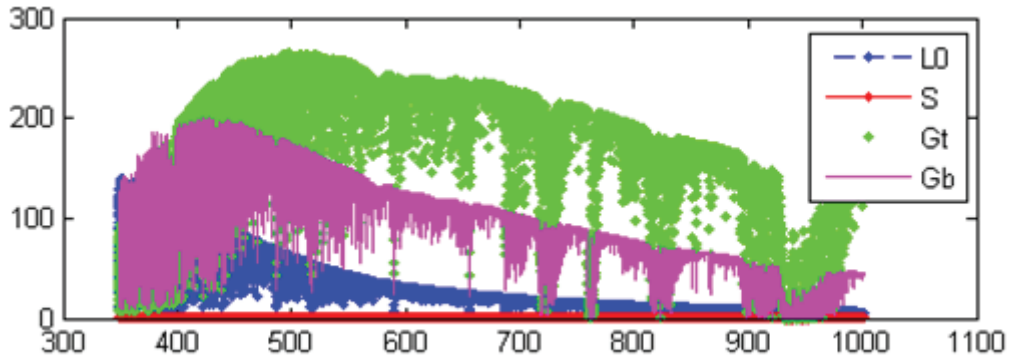

(a) Four atmospheric parameters L_0, S, G_t, G_b

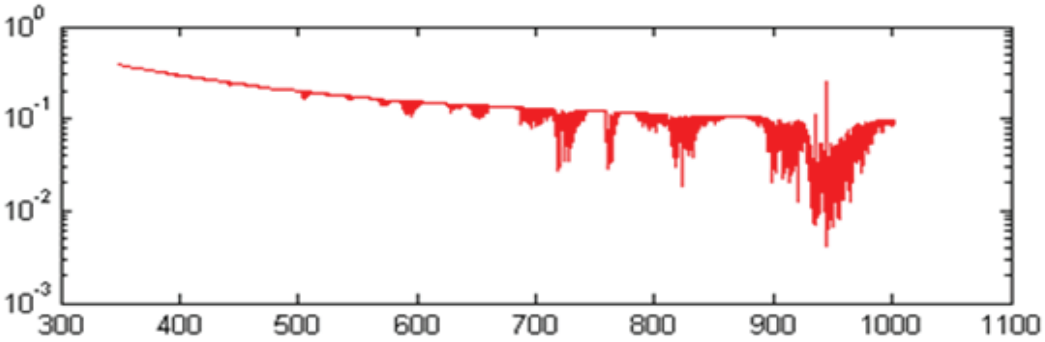

(b) S valus here are plotted again in oder to illustrate them more clearly

Figure 17 The atmospheric parameters L_0, S, G_t, G_b from MODTRAN simulation results using the MERIS L1 B image on 25 April 2008

3.3.2. Water leaving reflectance results by MODTRAN model and MERIS spectral response function

These four parameters of the MODTRAN simulation were computed for MERIS image bands by using Eq. (2.3.8) and shown in Fig. 18. Again, in order to see the S values clearly, S simulation values were plotted again in Fig. 18 (b).

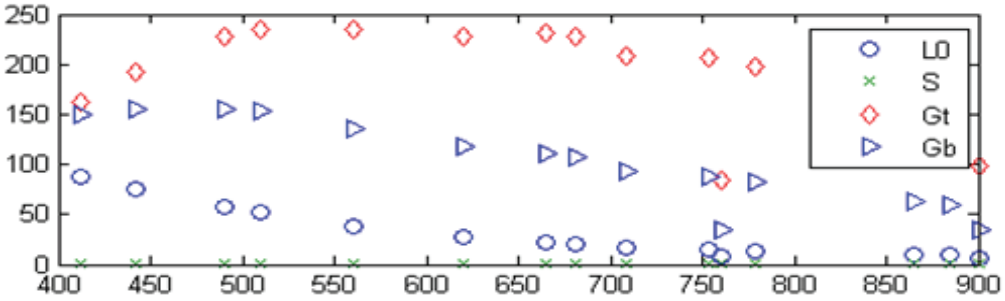

(a) Four atmospheric parametrs for MERIS bands L_0, S, G_t, G_b

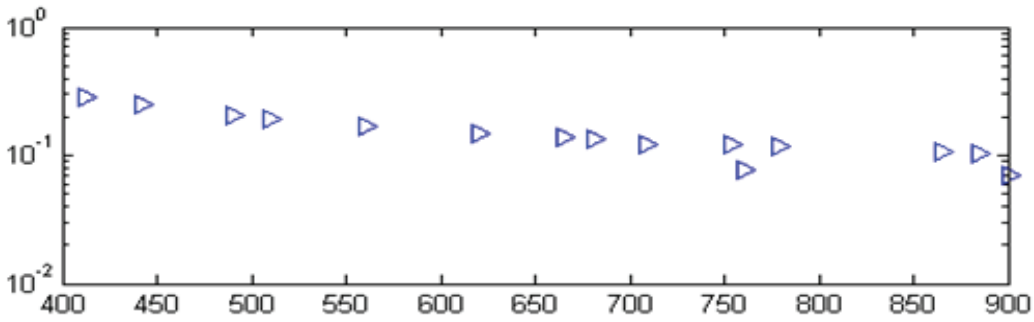

(b) *S* valus here are plotted again to illustrate them more clearly

Figure 18 The atmospheric parameters L_0, S, G_t, G_b for the MERIS L1 B image bands on 25 April 2008

Afterwards, Four atmospheric parameters L_0, S, G_t, G_b for the MERIS bands (in Fig. 18) and radiance from MERIS image on 25 April 2008 to calculate the water leaving reflectance using Eq. (2.3.6) in MATLAB script.

3.3.3. Sensitivity analysis of MODTRAN

Three atmospheric parameters visibility, view zenith and water vapor were changed with different values to show the atmospheric correction results. One pixel (PIN 1 chosen from the Fig. 22) is used as an example to show the simulated atmospheric correction results with different scenarios. Visibility ranged from 5 to 40 km. View zenith angle was set two values, 5 and 15, which are according to the MERIS image retrieval results. Water vapor was changed from 2.9 to 3.5 g/cm². The results are shown in Fig. 19.

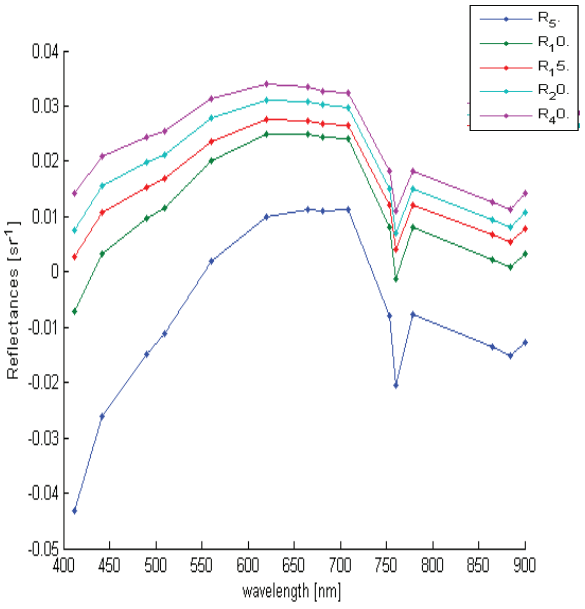

(a) Five scenarios with different visibility values

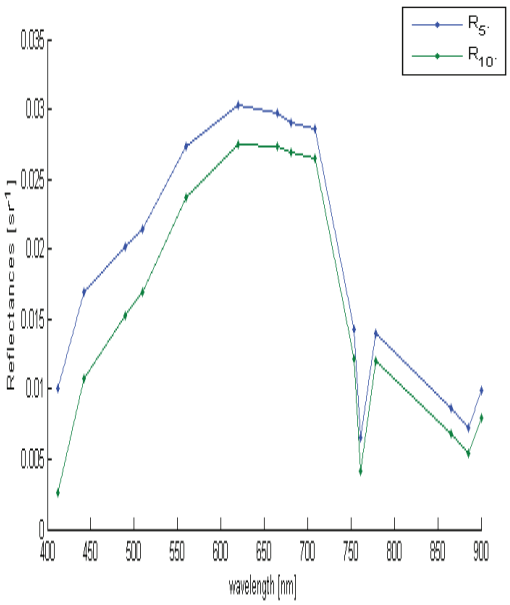

(b) Two scenarios with different view zenith angles (VIS = 15 km)

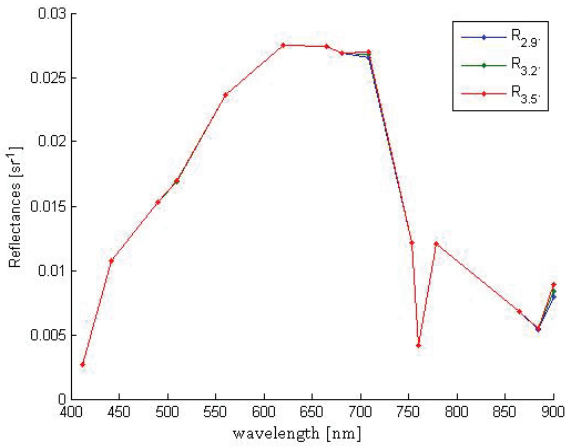

(c) Three scenarios with different water vapor concentrations (VIS = 15 km)

Figure 19 Water leaving reflectance retrieved from the MERIS L1 B image (Pin 1) on 25 April 2008 by the MODTRAN model for different visibility values, view zenith angles and water vapor concentrations

In Fig. 19, it is clear to see how these three parameters influence the water leaving reflectance. The visibility influences the reflectance most. The view zenith angle influences less than visibility. The water vapor just influences the reflectance results partly. The results show qualitatively that the visibility is the most influential parameter in my case, which determines the quality of atmospheric correction directly. View zenith angle influences the reflectance a little. Water vapor just influences the absorption bands (720 nm and 900 nm) and did not influence the reflectance a lot overall.

Then these input atmospheric parameters (Fig. 19) and also ozone concentration were analysed quantitatively to show how to influence the path radiance. The sensitivity analysis was calculated for some different MODTRAN input atmospheric parameters to obtain relative changes in radiances and are illustrated in Fig. 20 by using Eq. (2.3.1).

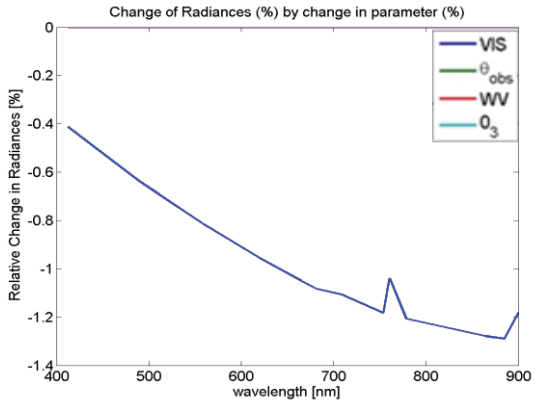

(a) visibility

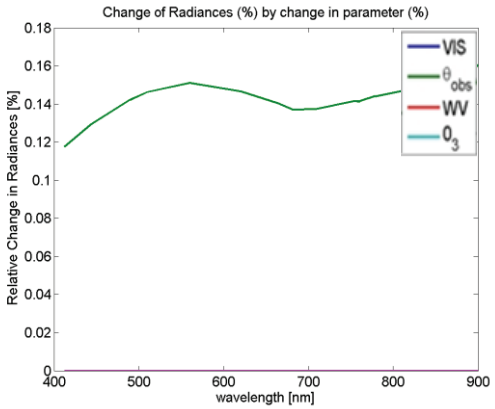

(b) view zenith angle

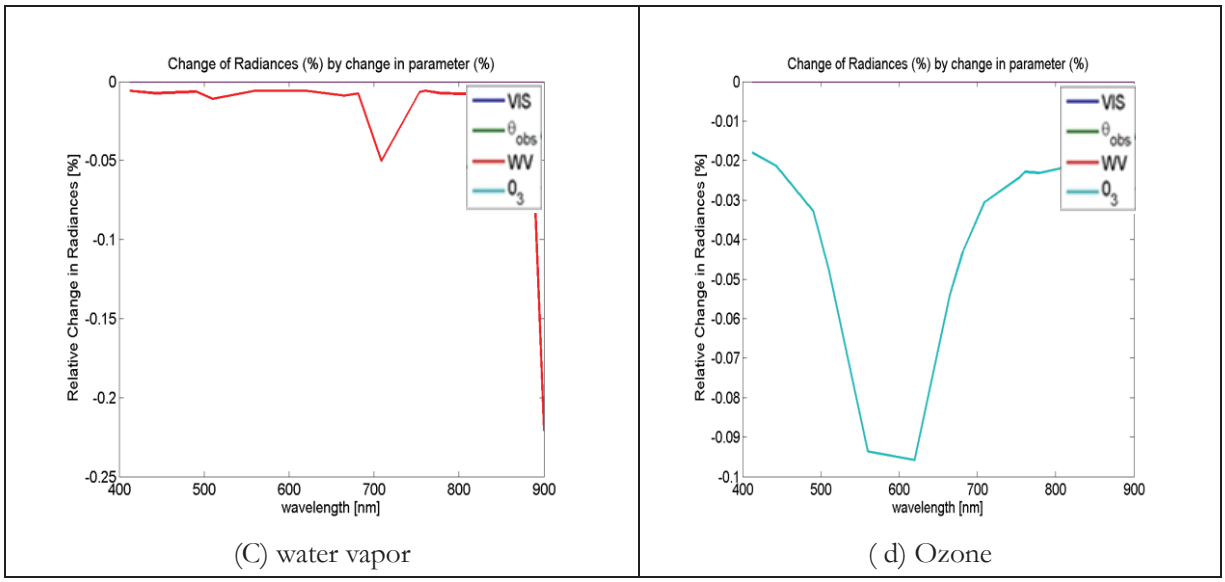

Figure 20 Sensitivity analysis of some MODTRAN input atmospheric parameters

In these four varied parameters shown in Fig. 20, visibility is the most influential parameter. The sensitivity increases as the band increases and the path radiance decreases as the band increases. But in the 760 nm and 900 nm bands, there are jumps that decrease the sensitivity due to the absorption of oxygen and water vapor. The view zenith angles changes less than visibility. The water vapor only influences the absorption bands around 720 nm and 900 nm a little. Ozone concentration changed little in my case.

Thus, one value for view zenith, water vapor and Ozone can be set as the input MODTRAN parameters and changed visibility form 5 to 40 (in Table 4) to simulate atmospheric parameters.

In this MERIS image on 25 April 2008, no evidence was founded for deviations from a homogeneous atmosphere. One pixel within the image can be chosen to calculate the water leaving reflectance by using four atmospheric parameters to perform the atmospheric corrected result. If it is reasonable, then the processing can be made in the same way for the whole study area. There are totally 15 scenarios in the MODTRAN simulation Look-up table. Here, one pixel (Pin 1 shown in Fig. 22) was chosen randomly as an example. The reflectance result has already been shown in Fig. 19 (c). Here, we did not illustrate it again. The result shows that the most reasonable visibility is 15 km and the best aerosol type is maritime. Due to a homogeneous atmosphere in my study area, the same atmospheric correction can be performed for the whole image.

3.3.4. C2RP products and comparing with MODTRAN simulation results

The atmospheric correction of the MERIS image on 25 April 2008 was also performed by the Case-2 regional processor in the BEAM software. It performed the atmospheric correction and the smile correction. The outputs are 12 water leaving radiance reflectances (not including 760 nm, 880 nm and 900 nm) for the whole scene. In Fig. 21, some of these bands (bands 3, 6, and 13) from the MERIS C2R processor product are shown below. In Fig. 22, 16 pixels were chosen randomly from different parts of the study. These 16 Pins were chosen with different ranges of SSC and were used to do the linear regression in section 3.5.

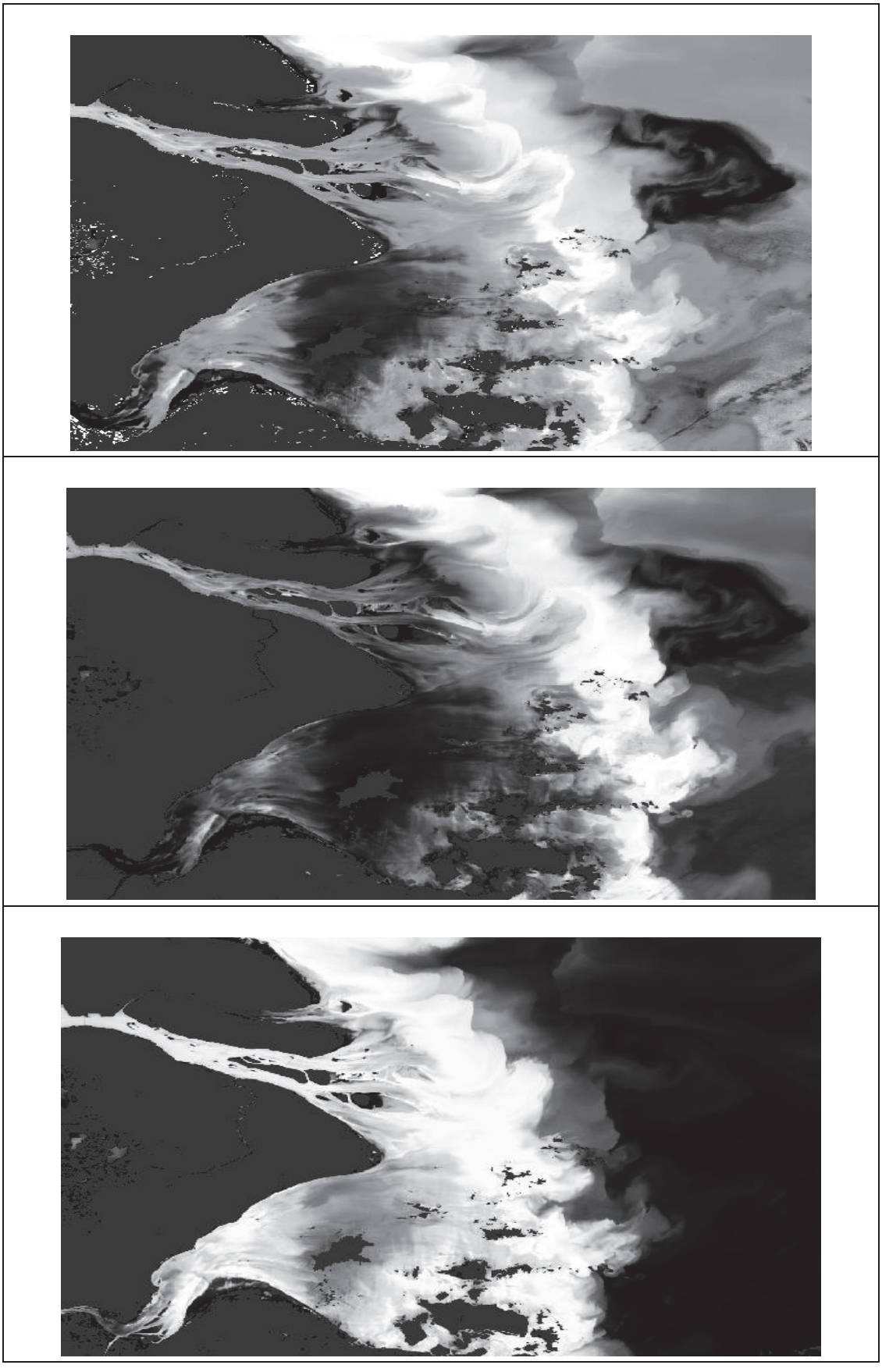

Figure 21 Atmosphericlly corrected MERIS products on 25 April 2008 (bands 3, 6 and 13)

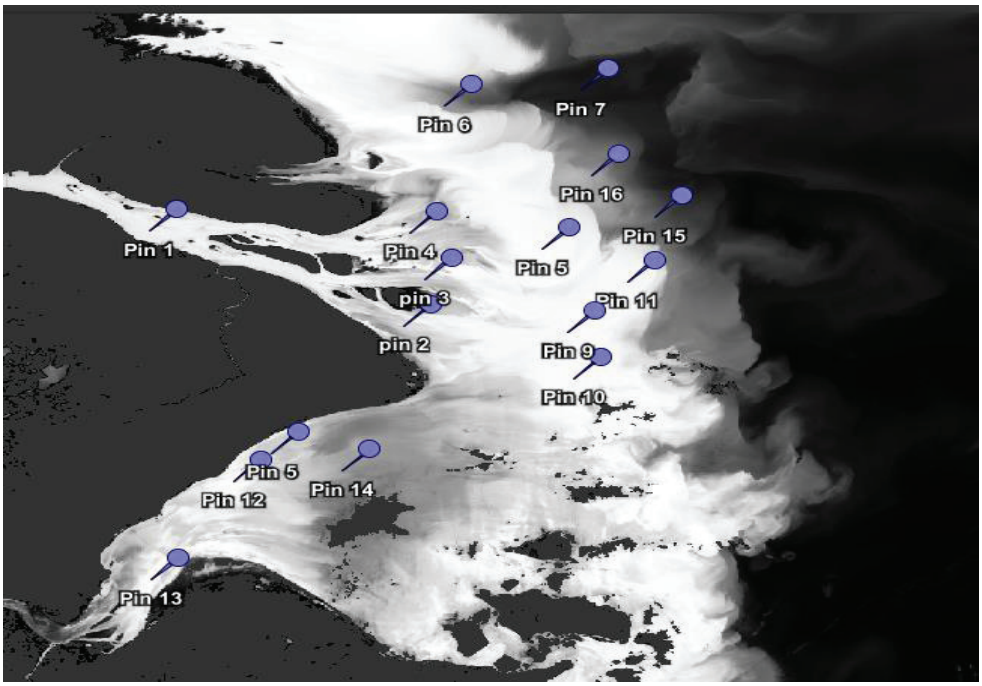

Figure 22 16 pins are shown in the Atmosphericlly corrected MERIS product on 25 April 2008 (band 9: 708nm) by C2R processor

3.3.5. Comparing Water leaving reflectance between the MODTRAN results and the C2RP results

After having got the atmospherically corrected product from C2RP, four pixels (pins 1, 2, 14, 6) from Fig. 22 were chosen to compare with the atmospheric correction results from MODTRAN.

The water leaving reflectance by C2RP in black and the water leaving reflectance by MORDTRAN in blue are shown in Fig. 23. Because C2RP just used 12 bands (not including 760 nm, 880 nm and 900 nm), the black curve is not continuous.

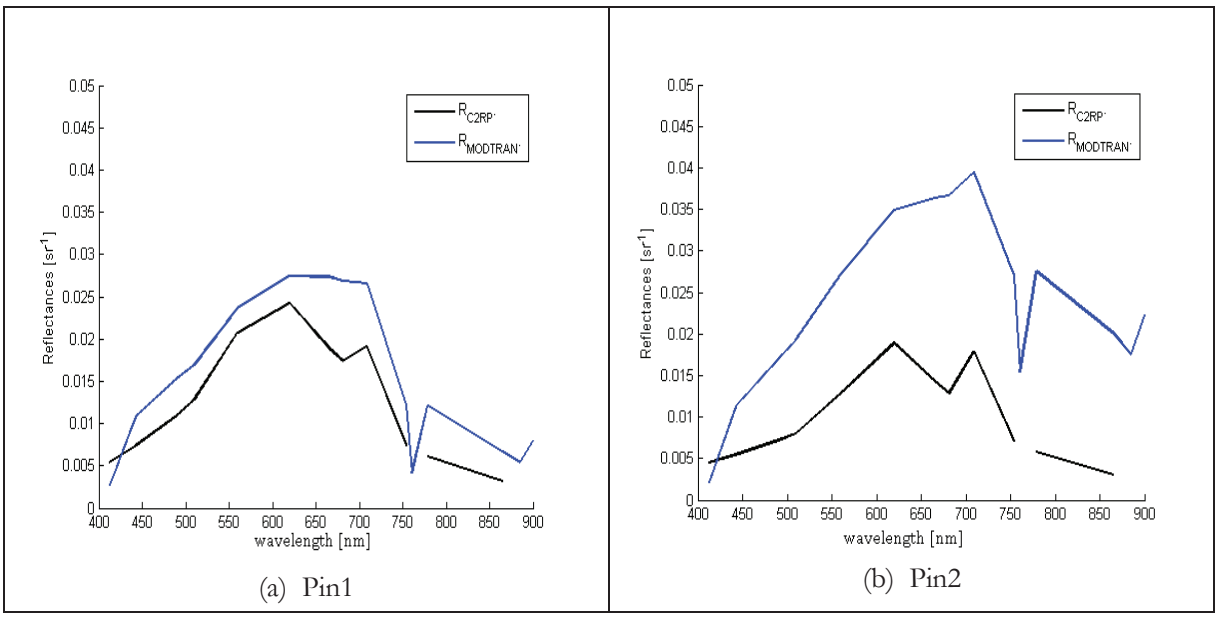

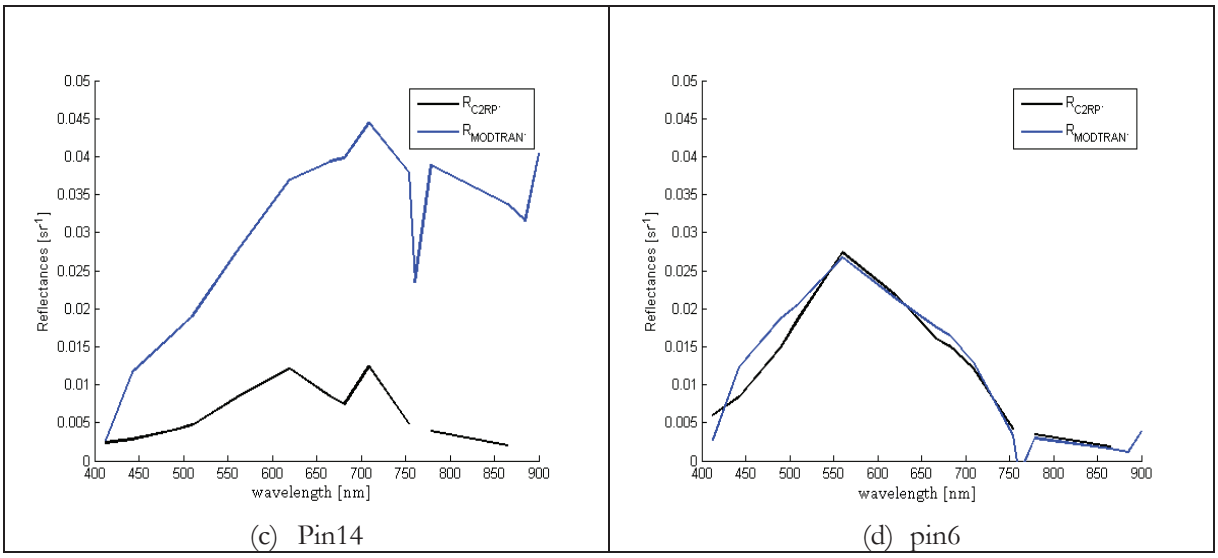

Figure 23 Comparing two reflectances from C2RP and MORDTRAN

In the results, it is easy to see that in a high sediment concentration areas (pin1, 2, 14), the reflectance by MODTRAN atmospheric correction model (in blue) showed differences with those by C2RP (in back), which were always higher than C2RP. This may be attributed to the presently used neutral networks (NN) in the C2RP, which have not been trained for the high SSC like found in the Yangtze River estuary and so this areas is out of scope of the C2RP. However, in clean water areas (pin6) with low sediment concentration, the two atmospheric correction results showed a lot of agreement.

According to the results, after comparison with Fig. 8, firstly, C2RP curves always shows lower values in high SSC (Pin1, 2, and 14) than MODTRAN curves and reference curves. Secondly, C2RP curves always show a dip at 680nm due to the Chl-a absorption. However, this dip does not appear in MODTRAN curves and reference curves.

From the results, it can be concluded that because of the limitation of the training data set of C2RP, C2RP is invalid for highly turbid waters but it makes sense for clean water. In my research, MODTRAN performed better than C2RP. C2RP basically underestimates high SSCs in this case. Besides, when comparing the simulated reflectance with the retrieved reflectance by MODTRAN and C2RP, we can also conclude that MODTRAN performed better than C2RP. These results are shown in section 3.4. In a nutshell, it is better to use the MODTRAN model to perform the atmospheric correction and then to retrieve the SSC for this research.

3.4. SSC retrieved results

3.4.1. SIOPs estimated results

After having derived water leaving reflectance based on the MODTRAN model and the C2R processor, those reflectances were first compared with the simulated spectral reflectance using the Duntley model and SIOPs that were chosen from the literature(Budhiman et al., 2012) directly. Four pixels (pin1, 2, 14,

6) were chosen with different levels of SSC. Simulated reflectances were estimated from a range of *S* based on Fig. 10. The results are shown in fig. 24.

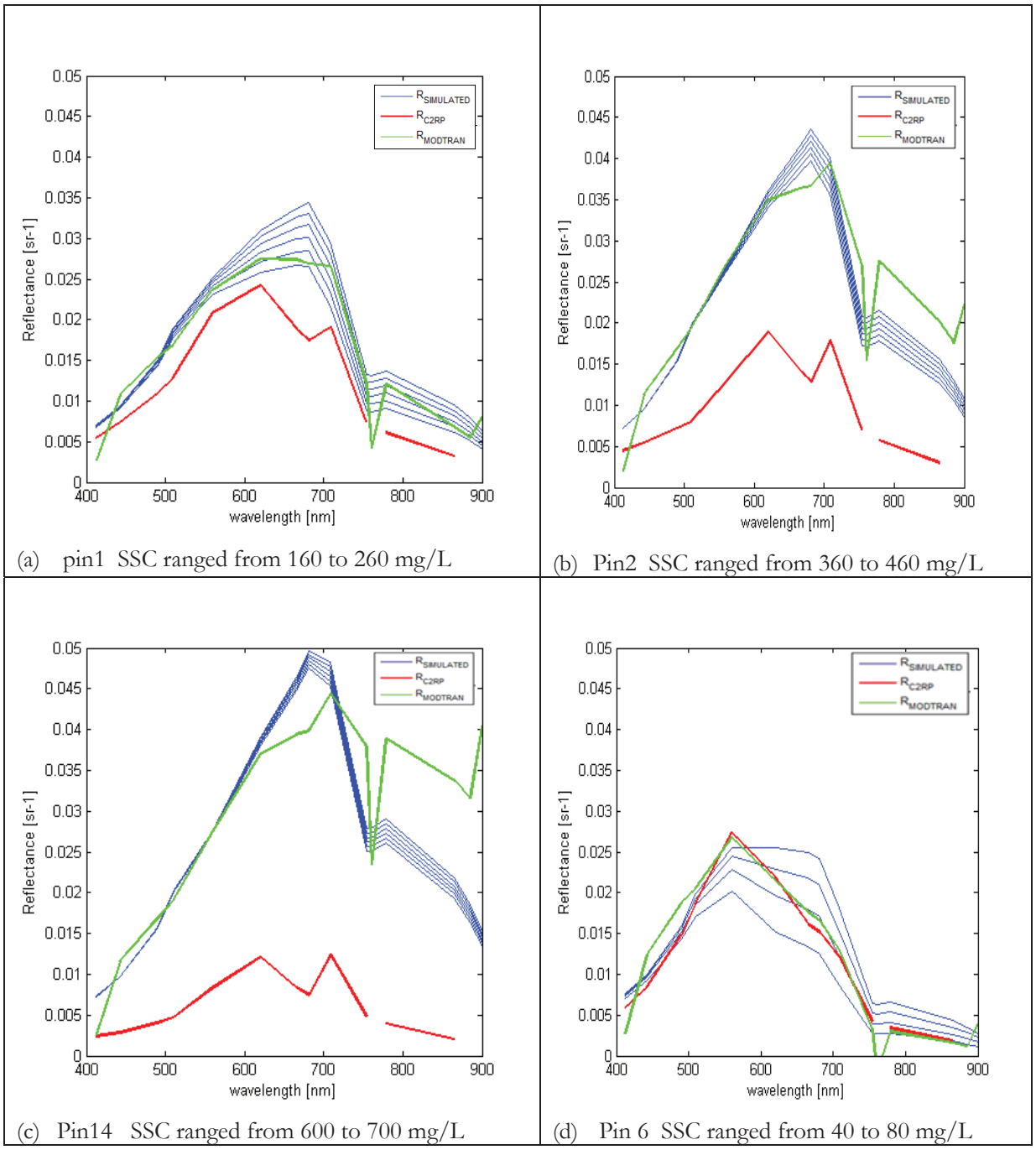

Figure 24 Comparing three reflectances from MODTRAN, C2RP and the simulated Duntley model with SIOPs from the literature

In Fig. 24, in turbid waters (pin1, 2, 14), retrieved results by MODTRAN showed more agreement with simulated results than the C2R processor. In clean water, all three reflectance curves showed a lot of agreement. The C2R processor always underestimated the reflectance in highly turbid waters but it makes sense in clean water. It can be concluded again (same in section 3.3.5) that the MODTRAN model is

better to use to retrieve SSC in my case. However, in the Fig. 24 (a), (b) and (c), the simulated curves did not match well with the retrieved curves by the MODTRAN model in turbid area. Firstly, the peak of the simulated reflectance always appeared at 680 nm, but the peak of the retrieved reflectance moved to higher bands with the increasing of the sediment concentration (in Fig. 24 (a), the peak is at 620 nm; in Fig. 24 (b) and (c) , the peaks are at 708 nm). Secondly, between 700 nm to 900 nm, in Fig. 24 (b) and (c), the retrieved curves values are much higher than the simulated curves values. It may due to the wrong SIOPs we used in Fig. 24. So the SIOPs values from literature (Budhiman et al., 2012) is not suitable in the Yangtze River estuary. It still needs to be improved.

Afterwards, according to the results (in Fig. 24), the SIOPs values should be updated, so that the simulated reflectance can better fit with the atmospheric corrected reflectance by the MODTRAN model. Here, one pixel in high turbid water and one pixel in clean water were chosen to determine two new groups of a_S values for both turbid water and clean water by using Eq. (2.4.22) and make the other constitutes of SIOPs equal to the literature. We assumed that the new SIOPs could improve the agreement of the atmospheric corrected reflectance by the MODTRAN model and the simulated Duntley reflectance in my case. The same four pixels (pin1, 2, 14, 6) were chosen like Fig. 24 and the results are shown in Fig. 25. Here, *S* values were also simulated in a range based on Fig. 10.

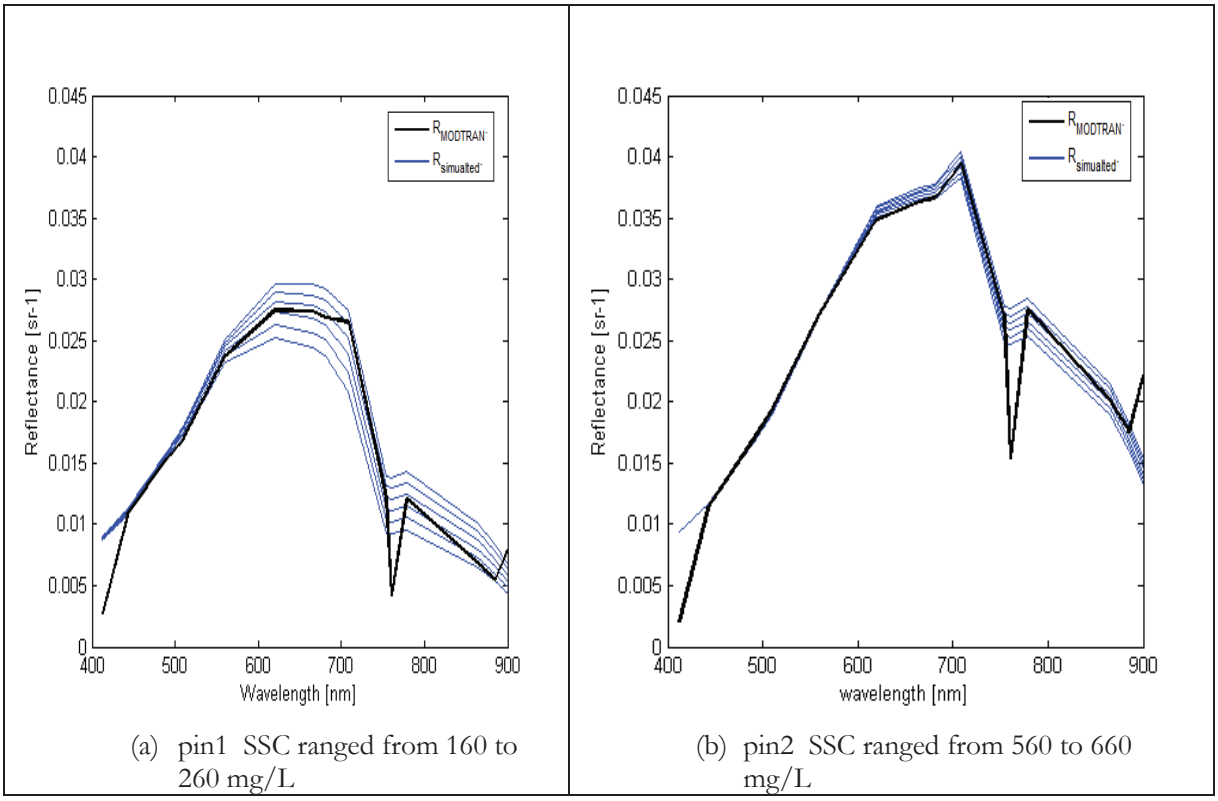

(a) pin1 SSC ranged from 160 to 260 mg/L

(b) pin2 SSC ranged from 560 to 660 mg/L

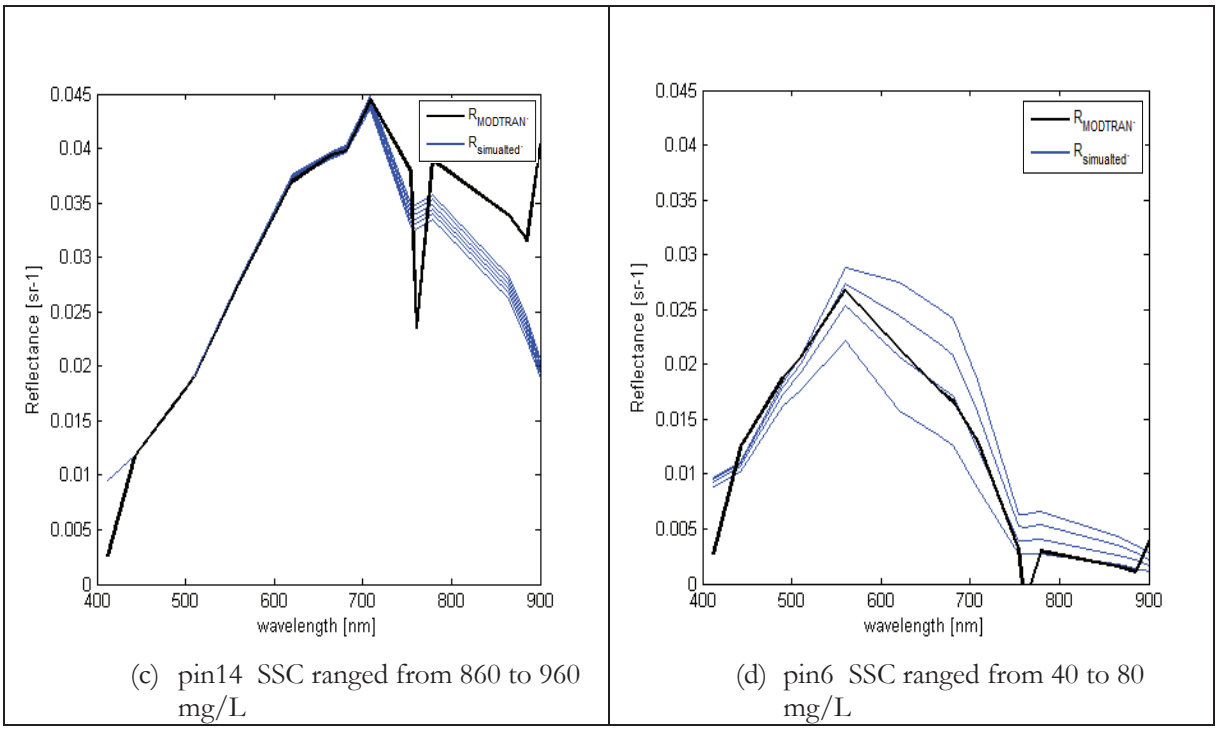

(c) pin14 SSC ranged from 860 to 960 mg/L

(d) pin6 SSC ranged from 40 to 80 mg/L

Figure 25 Comparing the retrieved reflectance from MODTRAN and the simulated Duntley reflectance with fixed SIOPs

From the results, we can see clearly that the fixed a_S showed better agreement in curve shape with the atmospheric correction results than a_S values chosen from the literature directly. The peaks from both simulated and retrieved curves always appeared in the same band. Especially between band 700 nm to 900 nm, the differences between simulated curves and retrieved curves became smaller than the results in Fig. 24. In short, the simulated reflectance result was quite improved by using the fixed SIOPs.

However, at 410 nm, 760 nm and 900 nm, these three bands from Duntley simulated reflectance showed always differences with the retrieved reflectance. Those at 760nm and 900nm bands are atmospheric absorption bands. The atmospheric correction results by MODTRAN showed a deep jump, where it should be smooth at 760 nm and 900 nm. This may be due to wrong oxygen concentration and water vapour concentration input parameters in MODTRAN. In the first band (410nm), the retrieved reflectance values were always lower than the simulated results. We cannot explain what the reason exactly is at this moment. However, even though these three bands (410 nm, 710 nm, 900 nm) are clearly in error and they cannot be fixed at this moment, it is not of influence on the final result because these bands were filtered out when retrieving the SSC values. Besides, band 1 cannot offer very useful information to retrieve SSC values in my case. Band 11 and band 15 just respond the oxygen concentration and the water vapor concentration. Thus, the error of these three bands cannot influence the final result of my research a lot.

In Fig, 25, these two simulated a_S values for turbid water and clean water improved the result a lot. The simulated a_S values should also fit to the exponential function in Eq. (2.4.21). The results are shown in Fig. 26.

Here, for the turbid water (area A), the spectral coefficient S=0.00837. For the clean water (area B), S=0.0059. From the literature, the spectral coefficient found S= 0.00196.

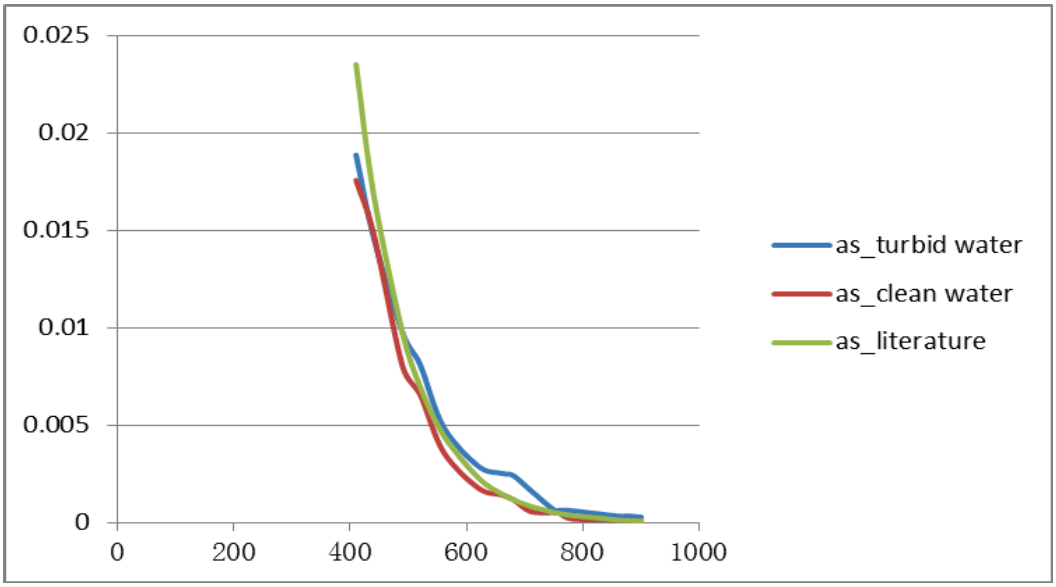

Figure 26 Spectral curves of a_S for two different areas (A and B) and one from the literature

3.4.2. SSC results by Duntley model

1. SSC retrieval algorithm

The simulated Duntley spectral curves were improved by estimating SIOPs in this case. Then the SSC can be retrieved for each pixel by using the inversion Duntley model.

Here, for turbid water and relatively clean water, two groups of a_S values were simulated, repetitively. Because the SSC values were retrieved for each chosen band and next calculated an average SSC. Choosing appropriate bands for the retrieval is important to guarantee the accuracy of the final SSC value.

From the atmospheric correction results in Fig. 25, at band 1, band 11 and band 15, the result showed obvious errors, so we further discarded these bands.

Here, we assumed that the other bands (except 1, 11 and 15) also influence the accuracy of the SSC value. Therefore, 5 pins (pin10, pin11, pin14, pin17 and pin 20) were randomly chosen with different levels of SSC and were analysed the fit between retrieved reflectance and simulated Duntley reflectance. The simulated reflectance was generated from the retrieved SSC value. The analysis was done by calculating absolute RMSE (Eq. 2.5.1) in Table 6.

Table 6 Multi-spectral bands relative accuracy analysis

Pin location	**Absolute RMSE**			**SSC mg/L**		
	Band 1-10, 12-14	Band1-10 and 12	Band 1-10	Band 1-10, 12-14	Band1-10 and 12	Band 1-10
Pin10	0.014498	0.01458	0.01459	195	201	210
Pin11	0.01996	0.02017	0.02098	312	350	367
Pin 8	0.01751	0.01862	0.01985	553	541	532

Pin14	0.01752	0.01863	0.02039	938	863	830
Pin20	0.01786	0.01795	0.0184	45.7	45.9	46.5

In the result, if some of the other bands are also excluded to from the retrieval, it did not change a lot, but still decreased the accuracy of the result a little.
Thus, the multi-spectral bands in this research were chosen to retrieve different ranges of SSC as below:

(1) SSC > 150, SIOPs for turbid water and bands 2-10 and bands 12-14 (without 1, 11 and 15) were used to retrieve SSC.
(2) SSC < 150, the other group of SIOPs for clean water and bands 2-10 and bands 12-14(without 1, 11 and 15) were used to retrieve SSC.

2. MERIS retrieval results

The SSC product next was generated for the whole study area from the atmospheric correction results by using MODTRAN model and the Duntley model in Fig. 27.
In Fig. 27, generally, the study area can be clearly divided into two parts: turbid area and clean water area. SSC has a wide range from 20 to more than 1500 mg/L. In area (1) South Branch, SSC has middle high values that ranges from 100 mg/L to 300 mg/L; in area (2) (3) (4) South Passage, North Passage and North Harbour, SSC has very high values that ranges from 300 mg/L to 800 mg/L; in area (5) Hangzhou Bay, SSC has super high values that ranges from 300 mg/L to more than 1500 mg/L.; in area (6) a transitional area, SSC has high values that ranges from 300 mg/L to 500 mg/L; in the area that is close to the coastal line, the SSC values increased more than 1500 mg/L; in area (7) clean water, from 122° 30' E to further, it is the relative clean water. SSC values are below 100 mg/L.

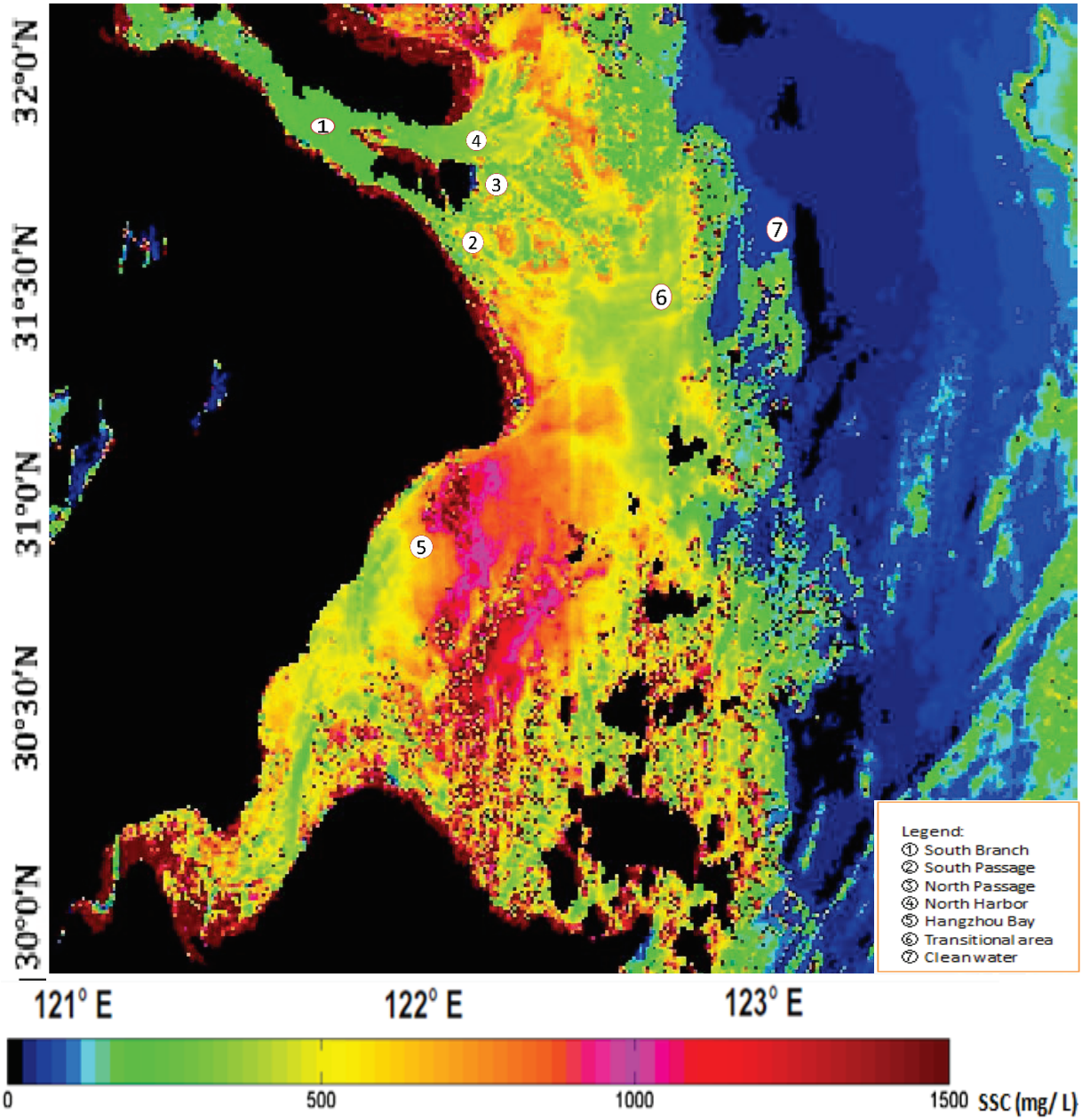

Figure 27 SSC product retrieved from MERIS L1B image on 25 April 2008 by using the MODTRAN model and the Duntley model

3. C2RP retrieval results

Case-2 regional atmospheric correction products (C2RP) were also used to retrieve SSC by the Duntley model and generated corresponding SSC product. The result is shown in Fig. 28. For the whole study area, SSC ranges from 20mg/L to 150mg/L. In the turbid region, SSC ranges from 30-100 mg/L, which is totally underestimated comparing with the reference SSC product and the SSC product in Fig. 27. In the region of clean water, SSC is below 50 mg/L, which is a better match with SSC products by using MODTRAN atmospheric correction model in Fig. 27. In Fig. 28, there is an area called 'M', which was explained in section 3.5 (4).

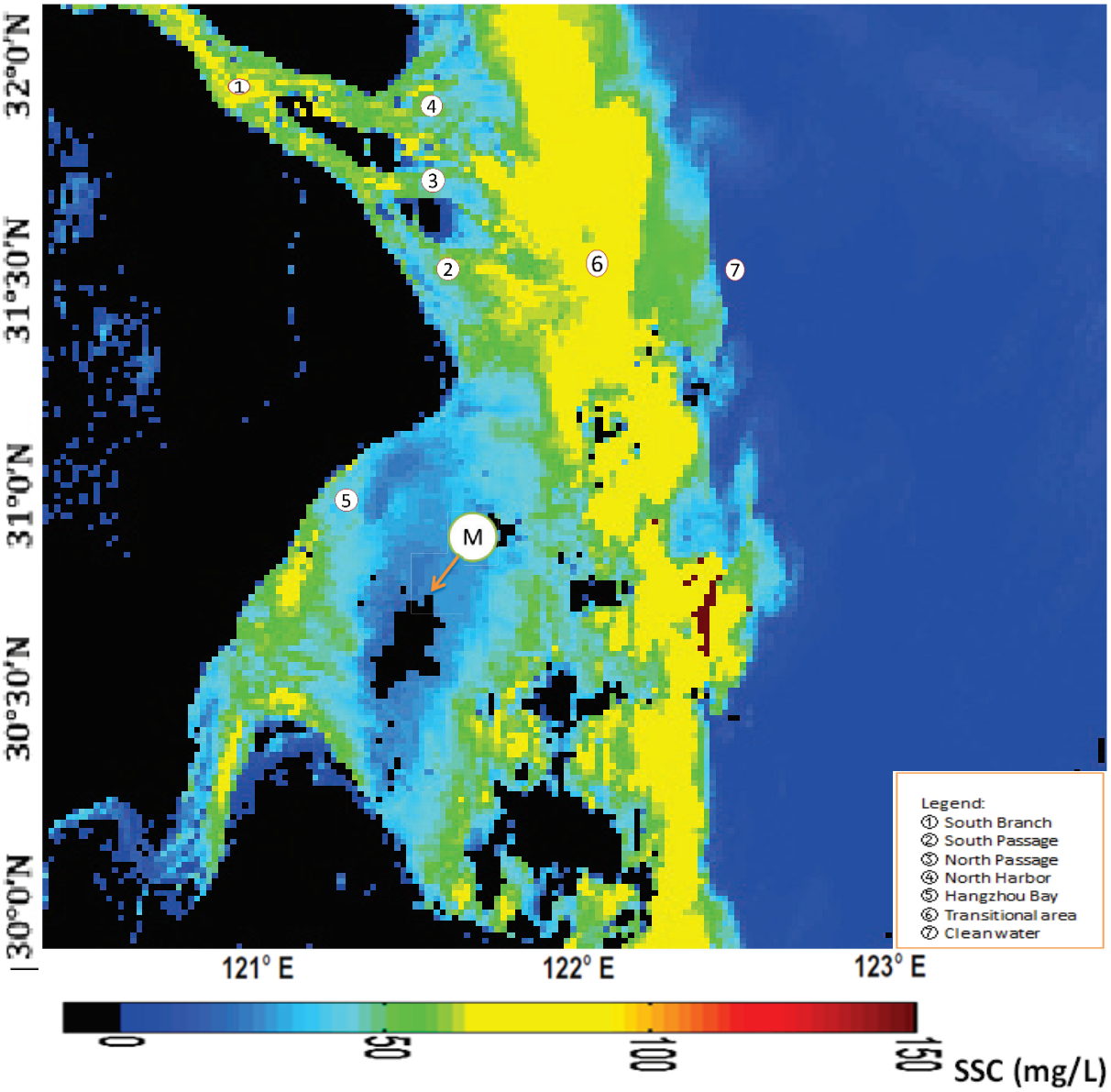

Figure 28 SSC product retrieved from MERIS L1B image on 25 April 2008 by using the C2R processor and the Duntley model

3.5. Evaluation results

3.5.1. The absolute RMSE calculation between simulated reflectance and MODTRAN retrieved reflectance

Five pixels (pin 1, 2, 5, 6 and 14) were chosen to retrieve SSC values and then generated corresponding simulated reflectance by the Duntley forward model. Here, the retrieved reflectance by the MODTRAN atmospheric correction model compared with the simulated forward Duntley reflectance by calculating the absolute RMSE (Eq. 2.5.1) between two curves in Table 7. In the result we can see that the simulated curves showed a good fit with the MODTRAN simulated results overall. The absolute RMSE is between 0.0099 - 0.019, which is very small overall.

Table 7 Absolute RMSE analysis between the retrieved curves by the MODTRAN model and the simulated curves by the Duntley water model in different pins

Pin location	Absolute RMSE	SSC mg/L
Pin1	0.009966	195
Pin2	0.014686	660
Pin5	0.015704	553
Pin6	0.019146	45
Pin14	0.017601	938

3.5.2. The relative RMSE calculation between simulated reflectance and MODTRAN retrieved reflectance

Since the reflectance value itself is very small, it would lead the absolute RMSE also very small. In order to show the differences between two reflectance curves more clearly, we next calculated the relative RMSE by using Eq. (2.5.2). From the previous results (Fig. 25), we can see that in band 1, band 11 and band 15, the differences are larger than the other bands. So here we calculated relative RMSE for all bands and without these three bands (band 1, 11 and 15). The results are shown in Table 8.

Table 8 Relative RMSE analysis between the retrieved curves by the MODTRAN model and the simulated curves by the Duntley water model in different pins

Pin location	Relative RMSE (all 15 bands)	Relative RMSE (without band 1, 11 and 15)	SSC mg/L
Pin1	0.723612	0.085812	195
Pin2	0.980758	0.034276	660
Pin5	0.768868	0.125803	553
Pin6	0.829885	0.310525	45
Pin14	0.71239	0.093296	938

According to the result, when excluding these three bands, the relative RMSE decreases dramatically. These three bands increase the relative error between retrieved reflectance and simulated Duntley reflectance. However, the results still showed a good fit between retrieved curve and simulated Duntely curve overall.

3.5.3. The linear regression

After having got the two SSC products, the same 16 pins according to Fig. 22 were chosen from both two SSC maps to analysis the linear regression. The result is shown in Fig. 29. The *X*-axis is log (SSC) from C2RP and the *Y*-axis is log (SSC) from MODTRAN. From the result, we can see two pins (pin 6 and pin 7) with low SSC values that showed agreement between C2RP SSC map and MODTRAN SSC map. The other pins with high SSC values showed totally different. Thus, we can once more conclude that the C2R processor is better to use in clean water and invalid for high turbid water such as the Yangtze River

estuary. The C2RP product is totally underestimating the high SSC levels since it was not trained for such high sediment concentration like those of the Yangtze River estuary.

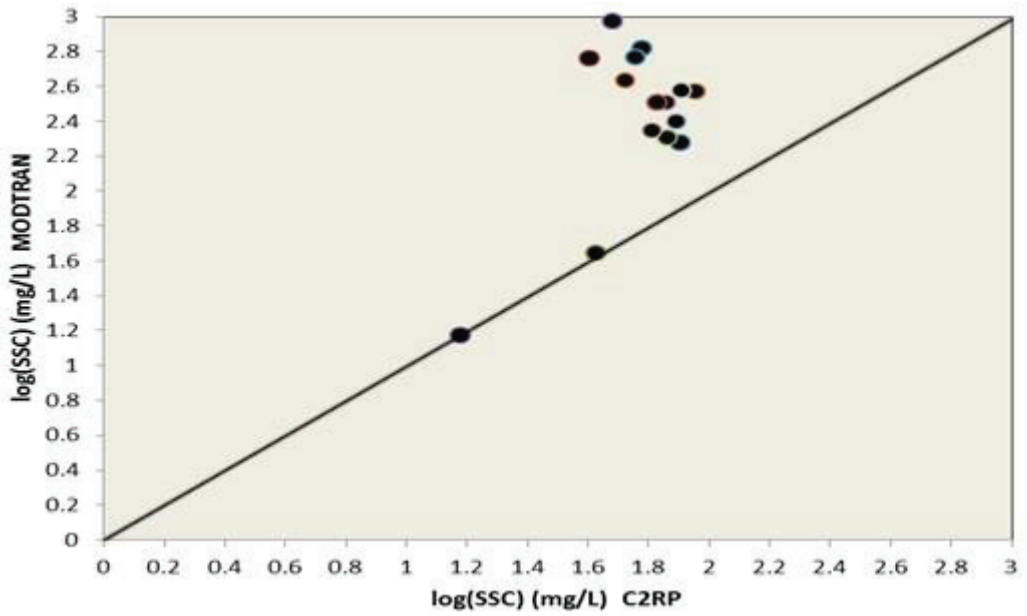

Figure 29 Comparison of SSC products retrieved by the Duntley model with two different atmospheric correction models MODTRAN and C2R processor using MERIS L1B data on 25 April 2008

3.5.4. Comparison with reference SSC product

The reference SSC product (Fig. 10) was generated by the atmospheric correction MODTRAN model and the SERT model by Shen, Verhoef, et al. (2010). In this research, two SSC products (Fig. 27 and Fig. 28) were generated by using the different atmospheric correction model: the MODTRAN model and the C2RP model and the same SSC retrieval algorithm: the Duntley water model. Due to the fact that we do not have the local data from the reference SSC product, limited ourselves to compare the differences and similarities from these three products below:

1. When comparing the SSC product (Fig. 27) by our model with the reference SSC product (Fig. 10), a lot of agreement could be found. They used the same atmospheric correction model. The SERT model is based on the K-M model and the Duntley model is also based on the K-M model but added the solar radiance. According to the result, most of the areas have the same levels of SSC in these two products. It means that when adding the solar radiance in the K-M model, there is not a big influence on the retrieved SSC values.
2. Next, all the three products were compared. It is clearly to see that the C2R processor is not suitable for the area with such high sediment concentration. Especially, in Fig. 28, we can see an area called 'M' where it showed negative values. It looks like haze or land. But in Fig. 10 and Fig. 27, in the same area, we do not see any land or spatially variable haze over this area. It just showed very high SSC values over 1000 mg/L. The C2R processor may even give wrong information more than wrong SSC values in highly turbid water.

4. CONCLUSION AND RECOMMENDATIONS

Up to now, not any research processed the atmospheric correction based on the spatially variable haze and used the Duntley water model to retrieve SSC by using two different sensors in the Yangtze River estuary. According to that, in this research, a new model to retrieve SSC based on the spatially variable haze were developed using MODIS and MERIS L1 images. In the result, firstly, we found that the MODIS bands signal is saturated because of the sun glint and high sediment concentration in water. Therefore, MODIS images are not suitable for my study area. Then when focusing on the MERIS images, no saturated signals were found with the MERIS scene. So MERIS images could be used in this research. Then the LUTs that contain four atmospheric parameters by the MODTRAN simulations based on the radiative transfer theory were generated. These four atmospheric parameters were used in the atmospheric correction to subsequently invert the water leaving reflectance from the MERIS L1 B image on 25 April 2008. Next, after having compared the retrieved reflectances by the MODTRAN atmospheric correction model with that form the MERIS L2 product by using the C2R processor, the MODTRAN model gave better results than C2RP. So, the retrieved reflectance by the MODTRAN model was next used to retrieve SSC by using the Duntley water model. The Duntley model is based on the radiative transfer theory in water which first links the water leaving reflectance with the water optical properties. Then the SSC values were parameterized by water optical properties and the specific inherent optical properties (SIOPs) by using the matrix inversion method. In this research, a new group of SIOPs were estimated, as the SIOPs from literature were found not suitable in this case. Then the simulated reflectances were generated from the retrieved SSC values using the updated SIOPs and these showed a good fit with the retrieved reflectances from MODTRAN. Therefore, finally a reasonable SSC map by using the MODTRAN atmospheric correction model and the Duntley model was generated.
The following conclusions can be drawn from the present result:

1. This model is suitable to retrieve a wide range of SSC values like the Yangtze River estuary.
2. The result of this model is considerably more accurate than the MERIS level 2 products by using the C2RP and shows a lot of agreement with the reference SSC products by using the SERT model in my study area.
3. In this research, one MERIS image on 25 April 2008 was used to retrieve SSC. In further studies, more images can be used to perform atmospheric correction under spatially variable haze and generate time series of SSC products from MERIS images.
4. In this case, the SSC product was based on setting CDOM and Chlorophyll-a concentrations as constant and just retrieving SSC values. This model developed in my research can be also applied to retrieve all the SSC, CDOM and Chlorophyll-a concentrations at the same time in further studies.
5. This developed model can also be used to other regions where the SSC levels need to be known. The group of the SIOPs values for other regions can be also estimated by using this developed model.

LIST OF REFERENCES

Barale, V. (1999). Ocean colour comes of age. *International Journal of Remote Sensing, 20*(7), 1197-1199. doi: 10.1080/014311699212687

Berk, A., Anderson, G. P., Acharya, P. K., Chetwynd, J. H., Bernstein, L. S., & Shettle, E. P. (1999). MODTRAN4 USER's MANUAL. *Hanscom AFB: Air Force Research Laboratory, Space Vehicles Directorate, Air Force Materiel Command,MA 01731-3010*.

Berk, A., Anderson, G. P., Acharya, P. K., Chetwynd, J. H., Bernstein, L. S., & Shettle, E. P. (2011). MODTRAN5 USER's MANUAL. *Hanscom AFB: Air Force Research Laboratory, Space Vehicles Directorate, Air Force Materiel Command,MA 01731-3010*.

Bricaud, A., Morel, A., & Barale, V. (1999). MERIS potential for ocean colour studies in the open ocean. *International Journal of Remote Sensing, 20*(9), 1757-1769. doi: 10.1080/014311699212461

Bricaud, A., Morel, A., & Prieur, L. (1981). Absorption by dissolved organic matter of the sea (yellow substance) in the UV and visible domains. *Limnology and Oceanography 26*(1), 43-53.

Budhiman, S., Salama, M. S., Vekerdy, Z., & Verhoef, W. (2012). Deriving optical properties of Mahakam Delta coastal waters, Indonesia using in situ measurements and ocean color model inversion. *ISPRS Journal of Photogrammetry and Remote Sensing, 68*(0), 157-169. doi: http://dx.doi.org/10.1016/j.isprsjprs.2012.01.008

Chen, S. L., Zhang, G. A., & Yang, S. l. (2003). Temporal and spatial changes of suspended sediment concentration and resuspension in the Yangtze River estuary. *Journal of Geographical Sciences, 13*(4), 498-506. doi: 10.1007/bf02837889

Chu, Z., Yang, X., Feng, X., Fan, D., Li, Y., Shen, X., & Miao, A. (2013). Temporal and spatial changes in coastline movement of the Yangtze delta during 1974–2010. *Journal of Asian Earth Sciences, 66*(0), 166-174. doi: http://dx.doi.org/10.1016/j.jseaes.2013.01.002

Craig, S. E., Lohrenz, S. E., Lee, Z., Mahoney, K. L., Kirkpatrick, G. J., Schofield, O. M., & Steward, R. G. (2006). Use of hyperspectral remote sensing reflectance for detection and assessment of the harmful alga, Karenia brevis. *Appl. Opt., 45*(21), 5414-5425.

Dai, S. B., & Lu, X. X. (2013). Sediment load change in the Yangtze River (Changjiang): A review. *Geomorphology*(0). doi: http://dx.doi.org/10.1016/j.geomorph.2013.05.027

Doerffer, R., & Schiller, H. (2007). The MERIS Case 2 water algorithm. *International Journal of Remote Sensing, 28*(3-4), 517-535. doi: 10.1080/01431160600821127

Doerffer, R., & Schiller, H. (2008). MERIS Lake Water Project—Lake Water Algorithm for BEAM ATBD. *GKSS Research Center 21502 Geesthacht*(Version 1.0).

Doxaran, D., Froidefond, J. M., Castaing, P., & Babin, M. (2009). Dynamics of the turbidity maximum zone in a macrotidal estuary (the Gironde, France): Observations from field and MODIS satellite data. *Estuarine, Coastal and Shelf Science, 81*(3), 321-332. doi: http://dx.doi.org/10.1016/j.ecss.2008.11.013

Doxaran, D., Froidefond, J. M., Lavender, S., & Castaing, P. (2002). Spectral signature of highly turbid waters: application with SPOT data to quantify suspended particulate matter concentrations. *Remote Sensing of Environment, 81*, 149–161.

Duan, H., Ma, R., & Hu, C. (2012). Validation of MERIS Case-2 Water Products in Lake Taihu, China. *GIScience & Remote Sensing, 49*(6), 873-894.

Duntley, S. Q. (1942). The Optical Properties of Diffusing Materials. *Journal of the Optical Society of America (1917-1983), 32*(2), 61-61.

Fettweis, M., Nechad, B., & Van den Eynde, D. (2007). An estimate of the suspended particulate matter (SPM) transport in the southern North Sea using SeaWiFS images, in situ measurements and numerical model results. *Continental Shelf Research, 27*, 1568–1583.

Gordon, H. R., Brown, O. B., Evans, R. H., Brown, J. W., Smith, R. C., Baker, K. S., & Clark, D. K. (1988). A semianalytic radiance model of ocean color. *Journal of Geophysical Research: Atmospheres, 93*(D9), 10909-10924. doi: 10.1029/JD093iD09p10909

Gordon, H. R., & Wang, M. (1994). Retrieval of water-leaving radiance and aerosol optical thickness over the oceans with SeaWiFS: a preliminary algorithm. *Applied Optics, 33*(3), 443-452.

He, Q., Yun, C. X., & Shi, F. R. (1999). Remote sensing analysis for suspended sediment concentration in water surface layer in Yangtze River estuary. *Progress in Natural Science (in Chinese with an English abstract), 9*, 160-164.

Hu, C., Carder, K. L., & Muller-Karger, F. E. (2000). Atmospheric Correction of SeaWiFS Imagery over Turbid Coastal Waters: A Practical Method. *Remote Sensing of Environment, 74*(2), 195-206. doi: http://dx.doi.org/10.1016/S0034-4257(00)00080-8

Ji, C. Y. (2008). Haze reduction from the visible bands of LANDSAT TM and ETM+ images over a shallow water reef environment. *Remote Sensing of Environment, 112*(4), 1773-1783. doi: http://dx.doi.org/10.1016/j.rse.2007.09.006

Jorgensen, P. V. (1999). Standard CZCS Case 1 algorithms in Danish coastal waters. *International Journal of Remote Sensing, 20*(7), 1289-1301. doi: 10.1080/014311699212731

Kopelevich, O. V. (1983). Small-parameter model of optical properties of sea waters. . *In: Monin, A.S. (Ed.), Ocean Optics, , vol. 1. Physical Ocean Optics, Nauka,*, 208-234.

Kubelka, P., & Munk, F. (1931). Ein beitrag zur optik der farbanstriche. *Z Techn Physik, 12*, 593-601.

Lee, Z., Carder, K. L., Mobley, C. D., Steward, R. G., & Patch, J. S. (1998). Hyperspectral Remote Sensing for Shallow Waters. I. A Semianalytical Model. *Appl. Opt., 37*(27), 6329-6338.

Lee, Z., Carder, K. L., Mobley, C. D., Steward, R. G., & Patch, J. S. (1999). Hyperspectral Remote Sensing for Shallow Waters. 2. Deriving Bottom Depths and Water Properties by Optimization. *Applied Optics, 38*(18), 3831-3843.

Li, P., Yang, S. L., Milliman, J. D., Xu, K. H., Qin, W. H., Wu, C. S., . . . Shi, B. W. (2012). Spatial, Temporal, and Human-Induced Variations in Suspended Sediment Concentration in the Surface Waters of the Yangtze Estuary and Adjacent Coastal Areas. *Estuaries and Coasts, 35*(5), 1316-1327. doi: 10.1007/s12237-012-9523-x

Salama, M. S., & Shen, F. (2010). Simultaneous atmospheric correction and quantification of suspended particulate matters from orbital and geostationary earth observation sensors. *Estuarine, Coastal and Shelf Science, 86*(3), 499-511. doi: http://dx.doi.org/10.1016/j.ecss.2009.10.001

Schroeder, T., Behnert, I., Schaale, M., Fischer, J., & Doerffer, R. (2007). Atmospheric correction algorithm for MERIS above case - 2 waters. *International Journal of Remote Sensing, 28*(7), 1469-1486. doi: 10.1080/01431160600962574

Shen, F., Suhyb Salama, M. H. D., Zhou, Y.-X., Li, J.-F., Su, Z., & Kuang, D.-B. (2010). Remote-sensing reflectance characteristics of highly turbid estuarine waters – a comparative experiment of the Yangtze River and the Yellow River. *International Journal of Remote Sensing, 31*(10), 2639-2654. doi: 10.1080/01431160903085610

Shen, F., & Verhoef, W. (2010). Suppression of local haze variations in MERIS images over turbid coastal waters for retrieval of suspended sediment concentration. *Opt. Express, 18*(12), 12653-12662.

Shen, F., Verhoef, W., Zhou, Y., Salama, M. S., & Liu, X. (2010). Satellite Estimates of Wide-Range Suspended Sediment Concentrations in Changjiang (Yangtze) Estuary Using MERIS Data. *Estuaries and Coasts, 33*(6), 1420-1429. doi: 10.1007/s12237-010-9313-2

Shen, F., Zhou, Y.-X., Li, D.-J., Zhu, W.-J., & Suhyb Salama, M. (2010). Medium resolution imaging spectrometer (MERIS) estimation of chlorophyll-a concentration in the turbid sediment-laden waters of the Changjiang (Yangtze) Estuary. *International Journal of Remote Sensing, 31*(17-18), 4635-4650. doi: 10.1080/01431161.2010.485216

Verhoef, W., & Bach, H. (2003). Simulation of hyperspectral and directional radiance images using coupled biophysical and atmospheric radiative transfer models. *Remote Sensing of Environment, 87*(1), 23-41. doi: http://dx.doi.org/10.1016/S0034-4257(03)00143-3

Wang, J. J., & Lu, X. X. (2010). Estimation of suspended sediment concentrations using Terra MODIS: An example from the Lower Yangtze River, China. *Science of The Total Environment, 408*(5), 1131-1138. doi: http://dx.doi.org/10.1016/j.scitotenv.2009.11.057